

Structural parameters of nearby emission-line galaxies

Miguel Sánchez-Portal¹ \star , Ángeles I. Díaz²,

Elena Terlevich^{3†}, Roberto Terlevich^{3,4}

¹ *Universidad Pontificia de Salamanca en Madrid, Paseo de Juan XXIII 3, 28040 Madrid, Spain*

² *Dpto. de Física Teórica, C-XI, Universidad Autónoma de Madrid, Cantoblanco, 28049 Madrid, Spain*

³ *Instituto Nacional de Astrofísica, Óptica y Electrónica, Tonantzintla, Puebla, México*

⁴ *Institute of Astronomy, Madingley Road, Cambridge, CB3 0HA, U.K.*

ABSTRACT

We present the results of an investigation on the main structural properties derived from *VRI* and H_α surface photometry of galaxies hosting nuclear emission-line regions (including Seyfert 1, Seyfert 2, LINER and starburst galaxies) as compared with normal galaxies. Our original sample comprises 22 active galaxies, 4 starbursts and 1 normal galaxy and has been extended with several samples obtained from the literature. Bulge and disc parameters, along with B/D relation, have been derived applying an iterative procedure. The resulting parameters have been combined with additional data in order to reach a statistically significant sample. We find some differences in the bulge distribution across the different nuclear types that could imply families of bulges with different physical properties. Bulge and disc characteristic colours have been defined and derived for our sample and compared with a control sample of early type objects. The results suggest that bulge and disc stellar populations are comparable in normal and active galaxies.

Key words: galaxies: active – galaxies: surface photometry – galaxies: morphology

1 INTRODUCTION

Global AGN host galaxy properties, including mass, luminosity concentration, morphological type, bulge-to-disc relationship, metal abundance and total luminosity, may influence nuclear activity and perhaps in turn be affected by it. It has been argued that there can exist a connection between nuclear activity and intense star formation episodes. While there are some observational indications that star formation is enhanced in circumnuclear regions of Seyfert galaxies (see for instance Hunt & Giovanardi 1992), other observations point in the opposite sense (e.g. Carone 1992). An outstanding, still controversial question is related to the fuel supply involving the transport of large quantities of mass from reservoirs located in the galactic disc (see for instance Shlosman et al. 1989); in this process the matter has to lose almost all of its angular momentum. This can be accomplished by gravitational torques produced by non-axisymmetric perturbations in the gravitational potential. These are associated either with interactions with companion galaxies or with structural features like bars, rings, oval distortions etc.

Current research on structural properties of galaxies

hosting nuclear activity is now largely concentrated in the near infrared (NIR) bands. There are several advantages in the use of the NIR for studying the host galaxy properties of AGNs: on the one hand, a normal stellar population is dominated by old red giants and therefore peaks around $1\mu\text{m}$. On the other, dust extinction is substantially reduced at these wavelengths. Therefore, the NIR is ideal to look for bars and morphological distortions that can be hidden by dust in optical wavelengths (e.g. Mulchaey & Regan 1997). Moreover, the contrast between stellar and non-thermal contributions is maximised, since the latter has a local minimum around $1\mu\text{m}$.

Hunt et al. (1997) performed NIR J , H , K broadband images and colours in a sample of 26 galaxies with $z \geq 0.015$ and found that the average colours, both of the outer and the inner discs, are independent of the activity class and equal to those of normal spiral galaxies. Outer disc colour gradients are also consistent with those of normal spirals. On the other hand, on a scale of a few kiloparsecs from the centre, starburst galaxies show ongoing star formation; in Seyfert 2 galaxies, they found evidence of “fossil” star formation activity a few hundred Myr old; finally, no evidence of star formation, either ongoing or fossil, exceeding that of a normal spiral, is found in Seyfert 1 galaxies. They infer an evolutionary starburst-Seyfert connection, although not so global and not so tight in time as previous studies implied.

\star e-mail: miguel.sanchez@upsam.net

\dagger Visiting Fellow, IoA, Cambridge

NIR structural parameter analysis from Hunt et al. (1999) shows that bulges of Seyfert and starburst galaxies follow very closely the trend defined by normal spiral bulges and elliptical galaxies. On the other hand, for a given disc effective radius, the mean surface brightness of the Seyfert discs is higher (by ~ 0.9 K mag arcsec $^{-2}$) than those of early-type spirals.

Márquez et al (2000) performed NIR J and K' broadband imaging and colours on nearby, isolated spiral galaxies either with an active nucleus (18 objects, either Seyfert 1 or Seyfert 2 according to Véron-Cetty & Véron 1993) or without it (11 galaxies). They state that global properties are similar in both active and non active galaxies, since both samples define the same bulge Kormendy relation between μ_e and r_e^{\dagger} and disc components also share the same properties (contradicting the result from Hunt 1999); they also found that bulge and disc scale lengths are correlated, with $r_{bulge} \approx 0.2r_{disc}$. On the other hand, NIR central colours of active galaxies are found to be redder than those of non active spirals, most probably due to the AGN light re-emitted by the hot dust and/or to the presence of active star formation in circumnuclear regions.

In spite of the advantages of the NIR region for such studies, optical wavelengths can still provide useful data; the use of the optical region has its own advantages: on the one hand, observers can benefit from the large size of current optical detectors, providing a convenient sampling of the galaxy disc; on the other, optical studies can rely on the large quantity of published data. Moreover, optical colour maps can be used as excellent tracers of the line emission regions present in AGNs and starburst galaxies (see, for instance Terlevich et al. 1991)

Early work from Yee (1983) using a SIT-vidicon camera has been followed by a large number of studies using CCD detectors. Mediavilla et al. (1989) and Pastoriza et al. (1989) performed VI broadband surface photometry on a sample of 13 Seyfert galaxies; they consider two classes: “bulge galaxies” and “disc galaxies” and found that the $V-I$ colour has a constant, equivalent value in both galaxy groups in the 3 Kpc aperture, indicating similar stellar populations, but outside the 5 Kpc aperture colours become bluer for disc galaxies and redder for bulge galaxies. Mediavilla et al. (1989) use the same sample to obtain bulge and disc parameters from the surface brightness radial profiles, finding that structural parameters are comparable to those of normal spirals and ellipticals.

MacKenty (1990) performed Kron-Cousins BVR CCD surface photometry of 51 Seyfert galaxies from the NGC and Markarian catalogs finding that in almost all cases, a mechanism to transport material to the nucleus is present (either bars or interactions); about one-fifth of the sample is composed by amorphous galaxies; some of them can be a remnant of past interactions. Colours and disc morphological parameters are in general similar to those found in normal spiral galaxies.

Xanthopoulos (1996) performed VRI CCD surface photometry of 27 Seyfert galaxies belonging to type 1, 2 and

intermediate categories, finding that: (a) generally, Seyfert galaxies are perturbed objects (either by bars or by interactions); (b) nearly half of the sample galaxies are barred; moreover, almost all of them present evidence of the existence of a mechanism to transfer material to the nuclear region; (c) all non-barred galaxies are either S0 or Sa; (d) Seyfert 1 and Seyfert 2 galaxies follow a very similar Hubble type distribution; Seyfert 2 galaxies tend to have redder nuclei; (e) Seyfert 1 and Seyfert 2 galaxies present the same disc colours. (f) colour gradients remain constant along both the bulge and the disc of the galaxy for both Seyfert types; (g) both types of Seyfert galaxy show the same range and dispersion of bulge and disc morphological parameters, and also similar bulge-to-disc luminosity ratios; the wide range of scale lengths observed in Seyfert galaxies may support their classification as early-type spirals. Moreover, the bulge and disc parameters of both Seyfert types are the same as those of normal early-type spirals.

Virani et al. (2000) performed R surface photometry on a sample of 32 Seyfert and 45 non active galaxies[§] from the CfA survey and derived bulge and disc morphological parameters from the azimuthally averaged surface brightness profiles. No statistically significant differences between the Seyfert and control samples are found in either morphological parameters or in light asymmetries (bars, rings, isophotal twisting, etc.), or even in the companion galaxies properties (magnitude, separation from the host, position angle relative to the host, magnitude difference between the companion and the host, strength of the tidal parameter). They conclude that the nearby environment of Seyfert galaxies is not significantly different from nonactive galaxies with the same morphological distribution.

Boris et al. (2002) performed BVI surface photometry on a sample of 10 Seyfert 1 galaxies along with narrow-band H_α images of a subsample of 6 objects. They found that morphologies are confined to early-type galaxies; half of them can be considered as compact; bars are found in only two cases; average $B-V$ colours are found bluer than those expected for this morphological type (perhaps due to the contribution of the active nucleus and/or the disc to the total luminosity). Evidence of tidal interactions is found in six objects of the sample. They obtain morphological parameters for the nucleus (gaussian), bulge and disc components finding that in most cases (six out of eight), the disc is best described by a truncated exponential profile. The cutoff is generally associated with the existence of reddened regions (probably dust in the inner few Kpc of the galaxy). Only one galaxy shows disc emission in H_α .

This paper presents a new optical study on the structural parameters of galaxies hosting nuclear emission-line regions. In order to overcome the usual weakness of this kind of studies (relatively small and frequently biased samples, uncertainties in the nuclear classification, specially in the control samples), whenever possible, we have tried to supplement our original sample with data from the literature, in particular morphological parameters, and to use an homogeneous, reliable nuclear classification from opti-

[†] Nevertheless, there is a difference in the slope of the Kormendy relation of active and non active galaxies at $\sim 2\sigma$ level that is not considered as relevant.

[§] From the control sample, at least two galaxies have been found to be active and at least five objects are nuclear starbursts according to Ho et al. (1997).

cal spectroscopy. When data from the literature is used, it is clearly indicated throughout. The paper is structured as follows: first, a description of the original sample and the adopted nuclear classification is outlined; second, a description of the bulge and disc decomposition procedure is given, followed by the results obtained; the discussion section then proceeds, including a thorough analysis of the structural parameters of galaxies hosting nuclear emission-line regions. Our analysis is closed with a discussion on the radial colour distribution of our sample objects. Finally, our conclusions are outlined in section 6.

2 THE SAMPLE

Our sample (described in Sánchez-Portal et al. 2000, hereafter Paper I) comprises 27 nearby galaxies in a wide range of Hubble types (from $T = -5$ to $T = 10$) and different level of nuclear activity.

The availability of an accurate and homogeneous nuclear classification is of critical importance when trying to determine the variation of the behaviour of a given physical property across a sample of galaxies with different degree of activity. To this end, in this paper we have modified the original nuclear classification from Paper I and adopted the nuclear types from Ho et al. (1997) (hereafter HFS), since it provides a reliable homogeneous framework. In addition to HII nuclei, Seyferts and LINERs, HFS recognises a group of “transition objects”, whose [OI] strengths are intermediate between those of HII nuclei and LINERs; transition objects can be most naturally explained as “normal” LINERs whose integrated spectra are diluted or contaminated by neighbouring HII regions. The HFS survey demonstrates that broad H_α exists not only in Seyfert 1 nuclei but also in LINERs and perhaps even in some transition objects. Accordingly, they propose to extend the “type 1” and “type 2” designations, along with the intermediate types (1.2, 1.5, 1.8 and 1.9) to LINERs and transition objects. Table 1 shows the old and current nuclear types. According to the adopted HFS classification, several nuclear types are different from the original ones presented in Paper I. Some objects experience a major modification: NGC 3998 and NGC 5077, formerly considered Seyfert galaxies, become LINERs, while M 106 and M 51, previously classified as LINERs are now included in the Seyfert category. NGC 6340 and NGC 6384, initially considered normal galaxies, fall now in the LINER class. Nevertheless, the main results outlined in Paper I are not affected.

3 BULGE-TO-DISC DECOMPOSITION PROCEDURE

A spiral or lenticular galaxy can be decomposed to a first approximation into a bulge and a disc. Despite several differences (e.g. greater rotational speed), bulges are generally considered as equivalent to elliptical galaxies due to their morphological similarity, surface brightness distribution and stellar content (Kormendy 1983). Therefore, the same analytical functions are used for ellipticals and bulges of spiral and S0 galaxies. Perhaps the most widely used fitting function is that from de Vaucouleurs (1948):

Table 1. Original and revised nuclear types. S = Seyfert, L = LINER, T = transition nucleus, SB = HII nucleus.

Galaxy	Old type	New type
NGC 3227	S1.5	S1.5
NGC 3516	S1.5	S1.2
NGC 3998	S1.5	L1.9
NGC 7469	S1	S1 ^a
NGC 4151	S1.5	S1.5
NGC 5077	S1	L1.9
NGC 6814	S1	S1 ^a
NGC 513	S2	S2 ^a
NGC 1068	S2	S1.8
Mrk 620 (NGC 2273)	S2	S2
Mrk 622	S2	S2 ^a
NGC 3982	S2	S1.9
NGC 5347	S2	S2 ^a
NGC 6217	S2	SB
NGC 7479	S2	S1.9
NGC 1052	L	L1.9
NGC 2841	L	L2
M 106 (NGC 4258)	L	S1.9
M 51 (NGC 5194)	L	S2
NGC 7177	L	T2
NGC 7217	L	L2
NGC 2146	SB	SB
NGC 3310	SB	SB
NGC 3353	SB	SB ^a
NGC 1023	Normal	Normal
NGC 6340	Normal	L2
NGC 6384	Normal	T2

^a Not present in the HFS catalog

$$I(r) = I_e 10^{-3.33[(r/r_e)^{1/4} - 1]} \quad (1)$$

where I_e is the intensity at r_e , the effective radius. The factor 3.33 is chosen so that half of the total light emitted by the model comes from inside r_e .

On the other hand, the disc component can be represented by an exponential law (Freeman 1970):

$$I(r) = I_0 e^{-(r/r_0)} \quad (2)$$

where I_0 is the disk central surface brightness and r_0 the disc scale length. Though the reason for an exponential surface brightness distribution is uncertain, it can be derived from a possible solution of the gravitational collapse of a uniform density rotating sphere (see for example, Freeman 1970, Kormendy 1983). Freeman (1970) distinguishes two types of galactic discs: *Type I* discs reach $r = 0$ while *Type II* do not, showing an inner cutoff. This can be due to an actual lack of mass with low angular momentum, perhaps in the protogalactic cloud, thus leaving a galactic disc with an inner “hole”. Alternatively, type II discs can be the result of the combination of a pure exponential disc plus an additional component like a lens (Freeman 1976). Kormendy (1977) proposed a formula to fit this kind of discs with internal cutoff, modifying the Freeman’s expression (eq. 2)

$$I(r) = I_0 e^{-[r/r_0 + (r_{cut}/r)^\beta]} \quad (3)$$

where usually $\beta = 3$.

Andredakis et al. (1995) have fitted the bulge profile with a generalised exponential profile of Sérsic (1968):

$$I(r) = I_0 e^{-(r/r_0)^{1/n}} \quad (4)$$

finding that the exponent n varies with the Hubble type; while for early-type spirals, $n = 4$ (standard de Vaucouleurs profile), late-type galaxies show exponential bulges (i.e. $n = 1$). Carollo et al. (1998) performed the analysis of HST WFPC2 F606W images of a sample of 75 spiral galaxies, ranging from Sa to Sbc. Only a fraction ($\simeq 40\%$) of the objects contains a smooth, classical $R^{1/4}$ bulge. The central structure of some sample objects presents an irregular morphology: it is often dwarf-irregular like; in a few cases is elongated, similar to a late-type bar. In several objects, the spiral structure reaches down to the innermost accessible scales. Occasionally, a small “bulge-like” feature coexists with the nuclear spiral structure. They found that, in several cases, these inner, morphologically-distinct structures are well fitted by an exponential profile. These exponential bulges embedded in the spiral structure appear to be fainter than $R^{1/4}$ bulges for a given total galactic luminosity and Hubble type.

Two basic methods have been customarily used for obtaining the bulge and disc components from the azimuthally-averaged surface brightness profiles: non-linear least squares fitting and iterative fitting. In the former method, a non-linear least squares algorithm is used in order to fit simultaneously both components, while in the latter, an iterative method is applied in order to fit both components independently: a linear least squares fit is applied first to the region dominated by one of the components; this first model is extrapolated to the whole range, and subtracted from the observed profile, giving a first estimate of the other component, and then the appropriate fitting law is applied, subtracting the obtained model from the observed profile. This residual is then fitted again and the procedure is repeated iteratively until convergence is achieved. The regions where each component dominates over the other should be estimated by visual inspection. Schombert & Bothum (1987) propose a combination of both procedures: first, an iterative procedure is used until convergence is achieved. The resulting bulge and disc parameters are then used as initial estimates for a non-linear least squares fitting procedure. de Jong (1996) has applied a two-dimensional method using two or three 2D components to model the bulge, disc and (whenever appropriate) bar and applying a non-linear algorithm capable of accepting different weights for each data point. An exponential bulge is proposed instead of the classical $R^{1/4}$ model.

In spite of the disadvantage of the subjective step of visual determination of the ranges of dominance of disc or bulge, we have chosen the iterative fitting procedure because it allows to control the evolution of the procedure and to exclude regions from the fitting if desired (e.g. regions dominated by a ring or lens, where the profile is not properly described by the sum of a bulge plus a disc). On the other hand, it is possible to detect a disc cutoff (i.e., type II discs). We have used as independent variable of the surface brightness profiles the equivalent radius, defined as $r_{eq} = \sqrt{A/\pi}$, where A is the area enclosed by a given isophote. The most accurate fittings are obtained when there exists a clear range of dominance of one component over the other, i.e. when

bulge and disc scale lengths are rather different. In those cases, the fitting has been always started by determining the disc dominance region. On the other hand, for those galaxies where a disc component never dominates, the fitting has been started by a bulge component. In those latter cases the fitting confidence depends on the accuracy of the $R^{1/4}$ law defining the bulge (Kent 1985). We have also computed the integrated bulge-to-disc luminosity ratio:

$$B/D \equiv \frac{\int_0^\infty I_{bulge}(r) 2\pi r dr}{\int_0^\infty I_{disc}(r) 2\pi r dr} = 3.61 \left(\frac{r_e}{r_0}\right)^2 \frac{I_e}{I_0} \quad (5)$$

where $I_{bulge}(r)$ and $I_{disc}(r)$ are the surface brightness distributions for bulge and disc given by equations 1 and 2. If the galaxy has a type II disc, equation 5 is no longer valid. Instead of using a fitting formula like equation 3 for this kind of discs, we have simply assumed that the galaxy has a sharp cutoff for certain radius $r = r_{cut}$. Therefore, we change the lower limit of the disc luminosity integral in equation 5, obtaining the expression:

$$B/D = 3.61 \left(\frac{r_e}{r_0}\right)^2 \frac{I_e}{I_0} \frac{e^{r_{cut}/r_0}}{\left(\frac{r_{cut}}{r_0} + 1\right)} \quad (6)$$

Our computation method assumes that, beyond certain distance from the galaxy centre, the effect of seeing on the surface brightness profile is negligible, and therefore the derived bulge and disc parameters are seeing-free. This assumption is supported by the calculations performed by Capaccioli & de Vaucouleurs (1983); they plotted the convolution function of the light distribution of an idealized E0 galaxy obeying the $R^{1/4}$ with a single gaussian seeing PSF, for different values of r_e and σ_{PSF} , and shown that there is a radius $r_{ini}(r_e, \sigma_{PSF})$ where the difference between the $R^{1/4}$ model and its convolved image becomes negligible. We have estimated r_{ini} using these curves and an initial guess of r_e and σ_{PSF} . Furthermore, we have tried to ensure that our computation is not contaminated by nuclear emission by checking the radial extension of the nuclear H_α emitting regions from our narrow-band surface photometry (see Paper I) and using as initial radius for profile fitting the maximum between r_{ini} and the radial emission extension.

4 RESULTS

Table 4 presents the resulting morphological parameters for the sample galaxies. Magnitudes have been corrected for inclination using the values from Paper I[¶]. The computation of profile data point errors is detailed in Paper I. Parameter errors presented here are those arising from the linear fitting procedure. Figure 1 shows the results of the bulge-disc decomposition in the I band. The whole set of surface brightness profiles is presented in Paper I.

[¶] $H_0 = 55 \text{ km s}^{-1} \text{ Mpc}^{-1}$ is used throughout the paper.

Table 2. Morphological parameters of the sample galaxies

Galaxy	Filter	r_e (") (Kpc)	μ_e (mag/'' ²)	r_0 (") (Kpc)	μ_0 (mag/'' ²)	B/D
NGC 3227	V	1.614 ± 0.136	18.267 ± 0.223	23.317 ± 0.630	20.56 ± 0.047	0.143
		0.165 ± 0.014		2.378 ± 0.064		
	R	1.745 ± 0.144	17.783 ± 0.217	23.313 ± 0.671	20.107 ± 0.047	0.172
		0.178 ± 0.015		2.378 ± 0.068		
	I	2.601 ± 0.070	18.144 ± 0.069	23.404 ± 0.511	19.546 ± 0.045	0.162
		0.265 ± 0.007		2.387 ± 0.052		
NGC 3516	V	8.948 ± 0.295	20.041 ± 0.066	21.447 ± 0.439	21.940 ± 0.036	5.354
		2.070 ± 0.068		4.962 ± 0.102		
	R	7.472 ± 0.217	19.269 ± 0.062	24.836 ± 1.385	21.875 ± 0.074	4.911
		1.729 ± 0.050		5.747 ± 0.081		
	I	8.491 ± 0.179	18.892 ± 0.043	18.314 ± 2.217	20.906 ± 0.219	8.212
		1.965 ± 0.041		4.238 ± 0.513		
NGC 3982	V	27.202 ± 1.417	22.512 ± 0.065	8.303 ± 0.266	18.631 ± 0.106	1.884
		2.662 ± 0.139		0.812 ± 0.026		
	R	21.741 ± 0.962	21.748 ± 0.058	8.288 ± 0.198	18.221 ± 0.077	1.677
		2.127 ± 0.094		0.810 ± 0.019		
	I	19.239 ± 0.189	20.963 ± 0.013	8.481 ± 0.241	17.874 ± 0.087	1.841
		1.882 ± 0.018		0.830 ± 0.023		
NGC 7469	V	2.062 ± 0.057	18.097 ± 0.065	30.772 ± 3.025	21.508 ± 0.102	0.375
		0.882 ± 0.024		13.161 ± 1.294		
	R	1.635 ± 0.029	16.904 ± 0.044	33.873 ± 7.090	21.652 ± 0.178	0.667
		0.699 ± 0.012		14.487 ± 3.032		
	I	1.609 ± 0.057	16.332 ± 0.088	15.399 ± 2.102	20.222 ± 0.239	1.419
		0.688 ± 0.024		6.586 ± 0.899		
NGC 4151	V	10.320 ± 0.987	20.001 ± 0.155	39.771 ± 2.080	20.985 ± 0.035	0.602
		0.907 ± 0.087		3.495 ± 0.183		
	R	6.100 ± 0.346	18.703 ± 0.102	27.596 ± 1.176	20.189 ± 0.043	0.693
		0.536 ± 0.030		2.425 ± 0.103		
	I	9.852 ± 0.222	18.921 ± 0.035	40.326 ± 2.155	19.947 ± 0.037	0.554
		0.866 ± 0.019		3.544 ± 0.189		
M 106 (NGC 4258)	V	12.732 ± 0.627	20.235 ± 0.079	62.609 ± 9.662	20.163 ± 0.114	0.140
		0.503 ± 0.025		2.472 ± 0.381		
	R	13.777 ± 0.609	19.966 ± 0.070	63.880 ± 7.346	19.783 ± 0.083	0.142
		0.544 ± 0.024		2.523 ± 0.290		
	I	14.787 ± 0.426	19.403 ± 0.044	57.365 ± 4.728	18.994 ± 0.067	0.165
		0.584 ± 0.017		2.265 ± 0.187		
NGC 6814	V	-	-	-	-	-
	R	2.386 ± 0.196	17.862 ± 0.204	20.509 ± 1.732	18.955 ± 0.159	0.134
		0.329 ± 0.027		2.826 ± 0.239		
	I	2.908 ± 0.353	17.523 ± 0.296	20.116 ± 0.104	18.320 ± 0.010	0.157
		0.401 ± 0.049		2.771 ± 0.014		
	I	-	-	-	-	-
Mrk 620 (NGC 2273)	V	1.990 ± 0.696	18.825 ± 0.918	11.676 ± 0.336	19.475 ± 0.062	0.191
		0.322 ± 0.112		1.893 ± 0.054		
	R	1.702 ± 0.165	17.829 ± 0.265	11.820 ± 0.458	19.102 ± 0.088	0.242
		0.276 ± 0.027		1.916 ± 0.074		
	I	1.677 ± 0.100	16.942 ± 0.156	11.787 ± 0.371	18.488 ± 0.069	0.304
		0.272 ± 0.016		1.911 ± 0.060		
Mrk 622	V	4.486 ± 0.113	20.807 ± 0.049	1.882 ± 0.105	16.110 ± 0.496	13.694
		2.754 ± 0.070		1.155 ± 0.064		
	R	3.787 ± 0.075	20.033 ± 0.040	2.340 ± 0.189	17.344 ± 0.584	15.330
		2.324 ± 0.046		1.436 ± 0.116		
	I	3.730 ± 0.085	19.496 ± 0.047	4.653 ± 0.871	19.869 ± 0.670	10.350
		2.290 ± 0.052		2.856 ± 0.535		

Table 2 – *continued*

Galaxy	Filter	r_e ($''$) (Kpc)	μ_e (mag/ $''^2$)	r_0 ($''$) (Kpc)	μ_0 (mag/ $''^2$)	B/D
M 51 (NGC 5194)	V	8.989 ± 0.805 0.36 ± 0.033	20.434 ± 0.151	17.811 ± 0.792 0.727 ± 0.032	17.992 ± 0.066	-
	R	7.371 ± 0.510 0.301 ± 0.021	19.786 ± 0.108	14.475 ± 0.582 0.591 ± 0.024	17.337 ± 0.056	-
	I	6.829 ± 0.600 0.279 ± 0.024	19.031 ± 0.153	14.421 ± 0.474 0.588 ± 0.019	16.714 ± 0.050	-
NGC 1052	V	38.554 ± 0.964 4.996 ± 0.125	21.918 ± 0.036	-	-	-
	R	35.321 ± 0.955 4.577 ± 0.124	21.287 ± 0.040	-	-	-
	I	28.426 ± 1.042 3.683 ± 0.135	20.285 ± 0.055	-	-	-
NGC 2841	V	33.019 ± 0.735 1.857 ± 0.041	21.513 ± 0.030	54.806 ± 12.437 3.082 ± 0.699	21.344 ± 0.151	1.121
	R	29.150 ± 0.456 1.639 ± 0.026	20.870 ± 0.022	49.690 ± 7.206 2.794 ± 0.405	20.726 ± 0.110	1.088
	I	26.658 ± 0.371 1.499 ± 0.021	20.052 ± 0.020	54.313 ± 2.231 3.054 ± 0.125	19.952 ± 0.026	0.793
NGC 3998	V	10.363 ± 0.267 0.973 ± 0.025	19.365 ± 0.048	17.987 ± 1.064 1.689 ± 0.100	20.173 ± 0.139	5.011
	R	9.627 ± 0.188 0.904 ± 0.018	18.797 ± 0.036	17.120 ± 1.099 1.607 ± 0.103	19.746 ± 0.157	5.734
	I	9.855 ± 0.178 0.925 ± 0.017	18.098 ± 0.033	17.404 ± 1.355 1.634 ± 0.127	19.079 ± 0.187	5.880
NGC 5077	V	16.889 ± 0.598 4.216 ± 0.149	21.201 ± 0.059	-	-	-
	R	15.385 ± 0.362 3.841 ± 0.090	20.468 ± 0.040	-	-	-
	I	15.355 ± 0.466 3.883 ± 0.116	20.095 ± 0.051	-	-	-
NGC 6340	V	9.251 ± 0.326 0.976 ± 0.034	20.486 ± 0.066	22.669 ± 0.325 2.392 ± 0.034	20.150 ± 0.029	0.441
	R	8.488 ± 0.238 0.896 ± 0.025	19.926 ± 0.054	22.088 ± 0.269 2.331 ± 0.028	19.756 ± 0.026	0.455
	I	8.610 ± 0.190 0.908 ± 0.020	19.227 ± 0.041	23.031 ± 0.340 2.430 ± 0.036	19.090 ± 0.030	0.445
NGC 6384	V	9.788 ± 0.352 1.435 ± 0.052	20.535 ± 0.072	27.015 ± 1.979 3.960 ± 0.290	20.619 ± 0.108	0.512
	R	2.981 ± 0.337 0.437 ± 0.049	17.768 ± 0.307	22.931 ± 1.645 3.361 ± 0.241	19.671 ± 0.143	0.352
	I	4.957 ± 0.245 0.727 ± 0.036	18.252 ± 0.118	21.506 ± 1.229 3.153 ± 0.180	19.138 ± 0.106	0.434
NGC 7177	V	12.885 ± 1.254 1.305 ± 0.127	20.913 ± 0.170	10.897 ± 0.210 1.104 ± 0.021	19.777 ± 0.057	1.772
	R	11.598 ± 1.018 1.175 ± 0.103	20.253 ± 0.158	11.588 ± 0.318 1.175 ± 0.032	19.580 ± 0.074	1.946
	I	6.547 ± 0.479 0.663 ± 0.049	18.575 ± 0.153	11.169 ± 0.325 1.131 ± 0.033	18.541 ± 0.083	1.202
NGC 7217	V	20.358 ± 1.611 1.697 ± 0.134	20.885 ± 0.121	19.623 ± 0.570 1.636 ± 0.047	19.220 ± 0.059	0.838
	R	30.241 ± 2.622 2.521 ± 0.219	20.878 ± 0.120	19.863 ± 0.648 1.656 ± 0.054	19.029 ± 0.065	1.525
	I	38.220 ± 2.514 3.187 ± 0.210	20.487 ± 0.086	17.819 ± 0.636 1.486 ± 0.053	18.481 ± 0.079	2.617

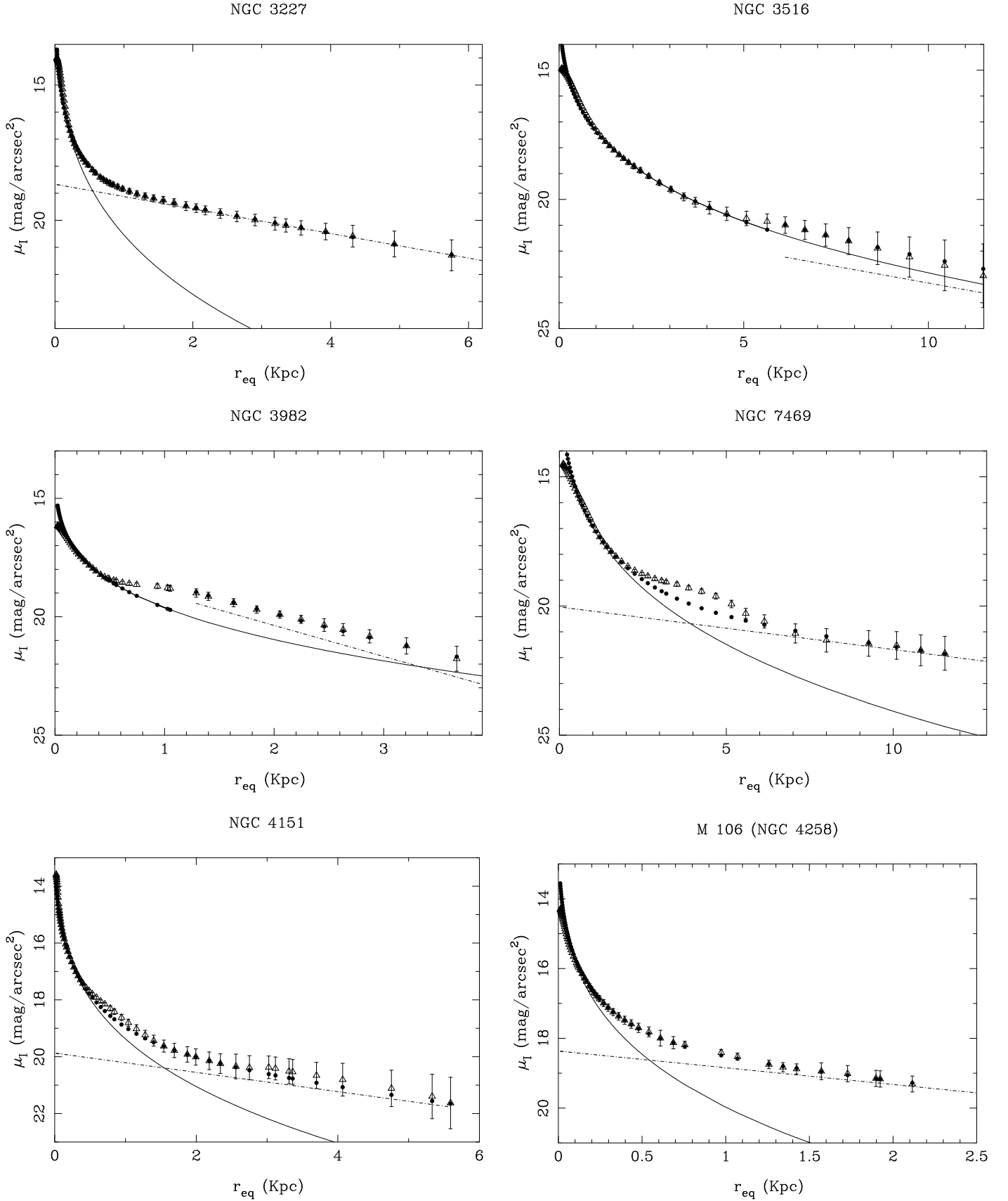
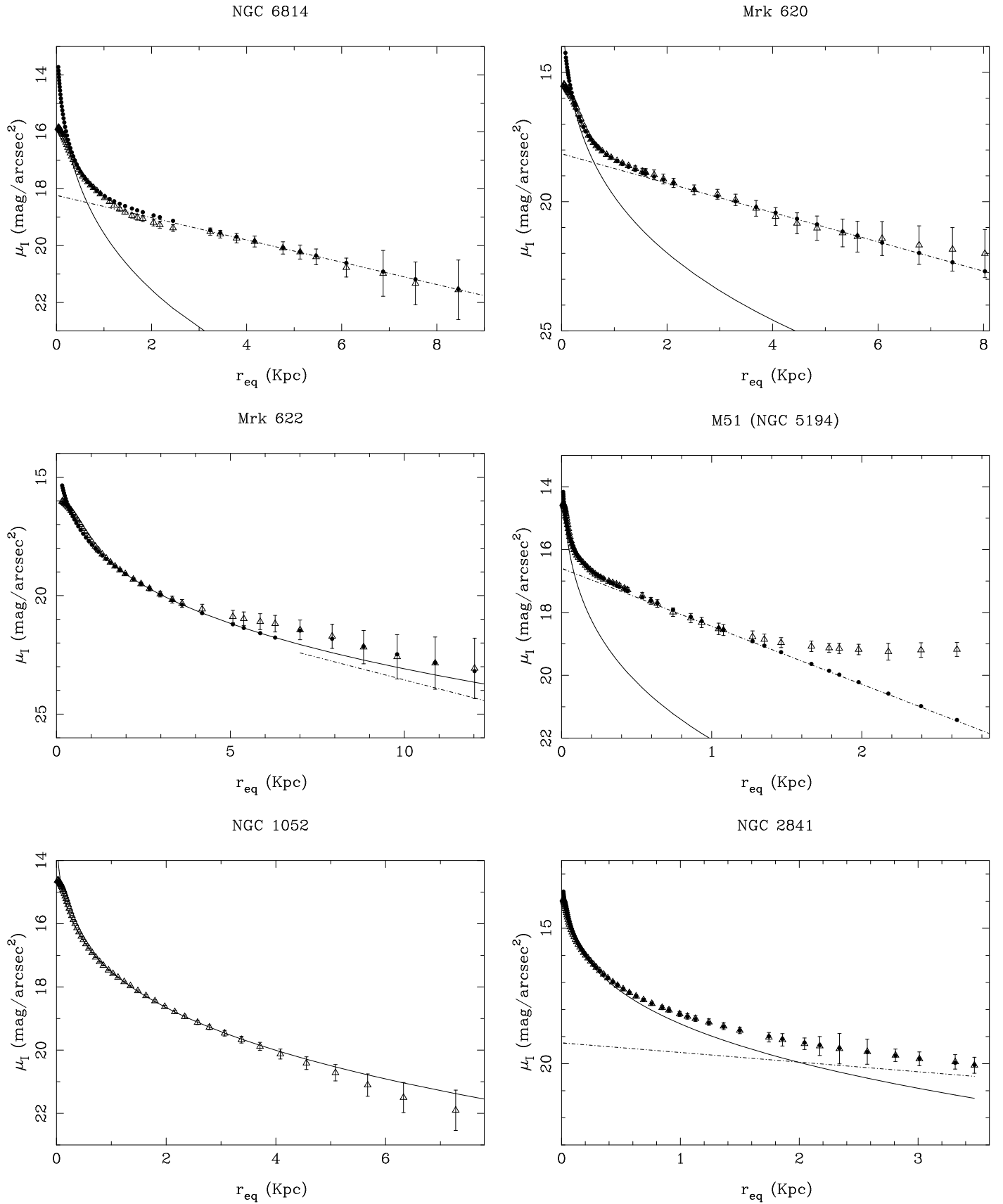


Figure 1. *I* band parameter decomposition. \triangle symbols represent the calibrated surface brightness profile, the solid line shows the bulge model, the dash-dotted line represents the disc model and \bullet symbols show the sum of bulge and disc models.

Figure 1 – *continued*

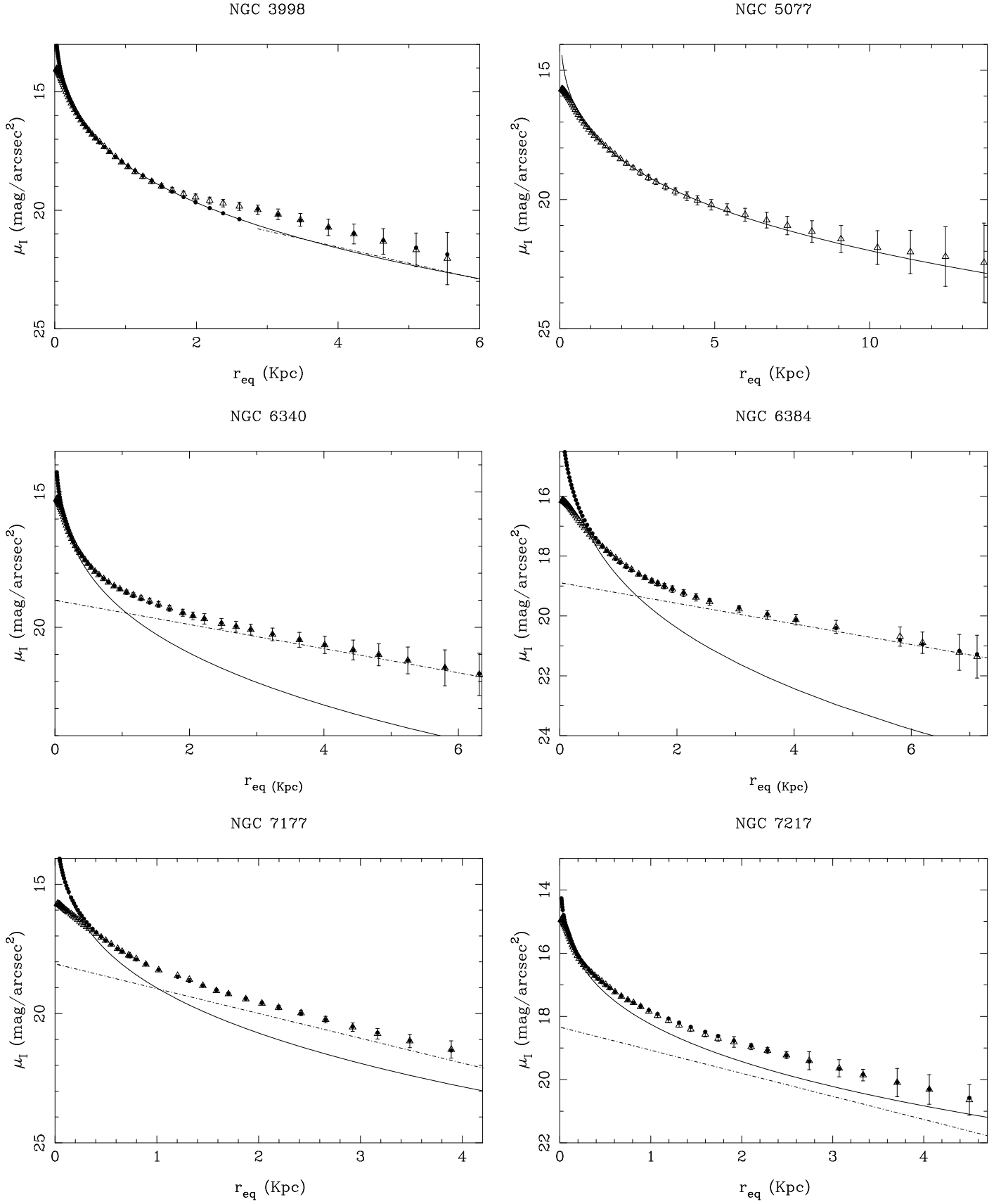


Figure 1 – continued

Table 2 – *continued*

Galaxy	Filter	r_e ($''$) (Kpc)	μ_e (mag/ $''^2$)	r_0 ($''$) (Kpc)	μ_0 (mag/ $''^2$)	B/D
NGC 2146	V	-	-	-	-	-
	R	-	-	-	-	-
	I	8.444 ± 1.322 0.665 ± 0.104	20.351 ± 0.278	20.136 ± 1.055 1.585 ± 0.083	19.173 ± 0.092	0.214
NGC 3310	V	1.950 ± 0.049 0.168 ± 0.004	18.431 ± 0.045	12.808 ± 0.637 1.106 ± 0.055	19.382 ± 0.185	0.201
	R	2.042 ± 0.211 0.176 ± 0.018	18.058 ± 0.187	13.346 ± 0.975 1.153 ± 0.084	19.245 ± 0.231	0.252
	I	2.563 ± 0.305 0.221 ± 0.026	17.932 ± 0.205	12.357 ± 0.567 1.067 ± 0.049	18.679 ± 0.175	0.309
NGC 6217	V	0.708 ± 0.019 0.085 ± 0.002	16.528 ± 0.084	21.276 ± 1.176 2.554 ± 0.141	20.137 ± 0.058	0.111
	R	1.425 ± 0.057 0.171 ± 0.007	17.818 ± 0.105	20.557 ± 1.035 2.468 ± 0.124	19.805 ± 0.054	0.108
	I	3.192 ± 0.109 0.383 ± 0.013	18.974 ± 0.075	20.353 ± 0.770 2.443 ± 0.092	19.276 ± 0.041	0.117
NGC 1023	V	21.680 ± 0.872 1.217 ± 0.049	20.627 ± 0.058	29.703 ± 1.879 1.667 ± 0.105	20.506 ± 0.062	1.721
	R	19.607 ± 0.673 1.101 ± 0.038	19.967 ± 0.051	27.754 ± 1.662 1.558 ± 0.093	19.979 ± 0.064	1.822
	I	19.731 ± 0.253 1.108 ± 0.014	19.333 ± 0.019	25.952 ± 0.903 1.457 ± 0.051	19.354 ± 0.040	2.127

4.1 Notes on individual objects

4.1.1 Seyfert 1.x galaxies

- NGC 3516: we have fitted to this SB0⁰ galaxy a Freeman type II disc^{||} with $r_{cut} = 5.7$ Kpc ($25''$)
- NGC 7469: a large excess for $2 \lesssim r \lesssim 6$ Kpc is observed in all the surface brightness profiles. Márquez & Moles (1994) attribute this feature to a lens structure, although they did not perform an accurate numerical fitting.
- NGC 4151: as already commented in Paper I, this spiral SABab presents a large-scale bar that affects the surface brightness profile from $r \sim 2.5$ Kpc outwards. Therefore, the disc profile is somewhat uncertain.
- NGC 6814: this SABbc galaxy presents a quite compact bulge. This fact, along with the relatively poor seeing ($\sim 2.3''$ FWHM) prevented us from obtaining V band morphological parameters. Márquez et al. (1999) observed this galaxy in the J and K' bands, finding bar parameters (PA , ϵ) very similar to ours (see Paper I). Nevertheless, the bulge and disc morphological parameters derived in the NIR are quite different to our optical parameters (though comparable): the bulge and disc equivalent radius lie between 9.2 arcsec and 62 arcsec in the J band and 5.5 arcsec and 40 arcsec in the K' band while our I band bulge and disc equivalent radius are equal to 2.9 arcsec and 33.8 arcsec, respectively.

^{||} As explained before, in all calculations throughout this paper, we have assumed a simplified type II disc with a sharp cutoff at r_{cut} .

- NGC 1068: an abrupt fall in the surface brightness profile (see Paper I) is observed at $r \approx 2.2$ Kpc, leading to an “inner” and an “outer” disc. Alternatively, this feature in the surface brightness profile can be attributed to the existence of a circumnuclear star-forming ring whose intensity peaks around 1.5 Kpc (Díaz et al. 2000). This fact, along with the poor seeing conditions during the observations ($\sim 2.2''$ FWHM) prevented us from performing an acceptable parameter decomposition.

- NGC 3982: this is the latest type (SABb) galaxy that presents a type II disc. We have applied a fit with $r_{cut} = 12''$.

4.1.2 Seyfert 2 galaxies

- NGC 513: in Paper I we classified this galaxy as SABa. We failed to perform a simple bulge+disc decomposition, but perhaps this galaxy owns a type II disc or additional components like a ring or lens.
- Mrk 622: according to Paper I, we classified this galaxy as SB0. We have fitted a type II disc with $r_{cut} = 11''$.
- M 51: the overall disc does not obey an exponential law. For $r > 40''$ the galaxy shows a flat profile, while for smaller radii the surface brightness distribution can be fitted to an exponential profile with small scalelength. This behaviour has been also reported by Boroson (1981), who finds a flat disc for $r > 52''$. The shape of the surface brightness profile can be explained by the presence of a nearby companion galaxy, NGC 5195.
- NGC 5347: the outstanding bar present in this SBab

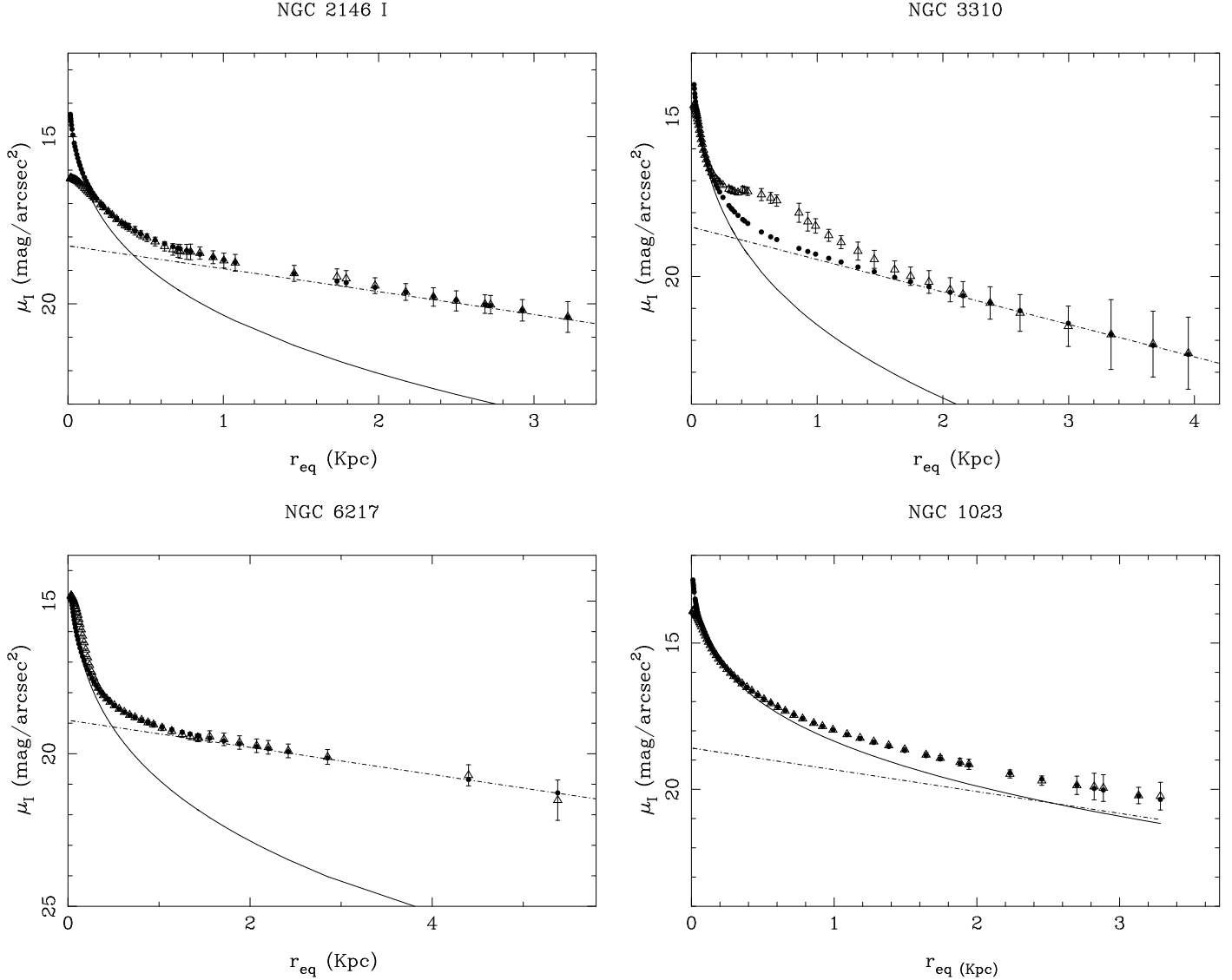


Figure 1 – continued

galaxy made impossible to perform a bulge+disc parameter decomposition. The K' image from Márquez et al. (1999) only shows a large bar also observed in our optical images. Their NIR bar parameters (PA , ϵ) match our optical parameters (Paper I). They are able to derive bulge and disc morphological parameters: the bulge and disc equivalent radius lie between 7.9 arcsec and 23 arcsec, respectively, in the J band and 2.2 arcsec and 19 arcsec in the K' band.

- NGC 7479: as in the previous case, this SBc has a very strong bar that dominates the surface profile. Therefore, it was not possible to perform an acceptable parameter decomposition.

4.1.3 LINERs

- NGC 3998: we have fitted to this SA0⁰ galaxy a Freeman type II disc with $r_{cut} = 2.75$ Kpc (30").
- NGC 5077: this E3-4 galaxy is the main member in a group of eight; a luminosity excess (halo) is detected from $r \sim 5$ Kpc outwards (figure 1).

- NGC 7177: the surface brightness profile lies below the $R^{1/4}$ law for $r < 3.8''$; this behaviour cannot be explained in terms of a seeing effect: we have computed the expected light distribution for a pure $R^{1/4}$ bulge with $r_e \approx 6.5''$ convolved with the same seeing PSF (about 1.2"FWHM) finding that the expected profile flattening begins about $r \approx 0.65''$. Therefore, the observed flattening seems to be an intrinsic bulge characteristic.

5 DISCUSSION

5.1 Bulge and disc parameters of active and normal galaxies

5.1.1 The extended sample

In order to perform a detailed study of the behaviour of bulge and disc parameters across all levels of nuclear activity, we have increased our sample by compiling from the literature a large number of morphological parameters be-

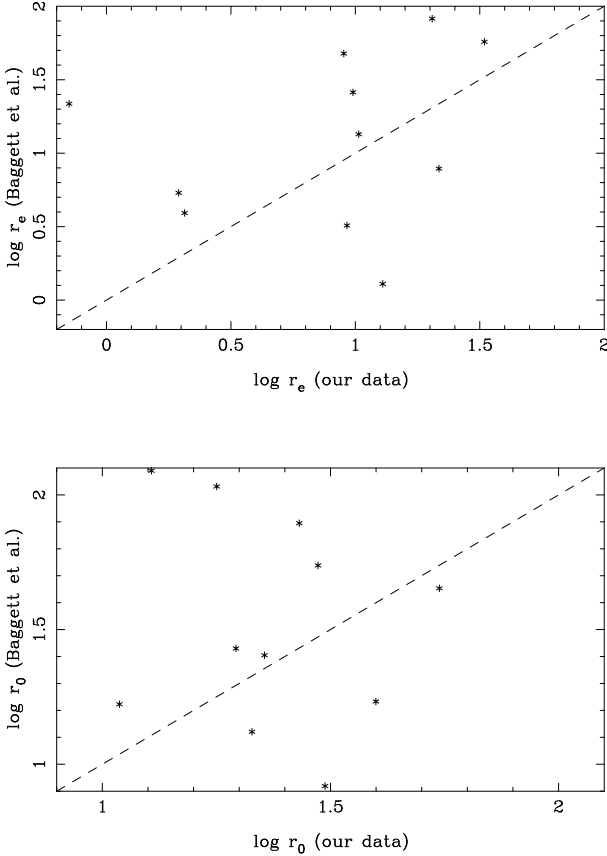


Figure 3. Comparison between disc (r_0) and bulge parameters (r_e) from our data and BBA data.

longing to galaxies contained in the HFS catalog. Our main source of data is the set of bulge and disc parameters from Baggett et al. (1998) (hereafter BBA) that comprises 659 galaxies, from which we have selected bulge and disc parameters for the 234 objects contained in the HFS catalog.

The extended sample contains 261 galaxies hosting all levels of nuclear activity. According to the classification of HFS the sample contains 22 Seyfert 1, 16 Seyfert 2, 90 LINERs, 108 starburst and HII galaxies and 25 normal galaxies. Therefore, there is an excess of low-activity nuclei.

BBA parameters were derived using profiles obtained from major axis cuts of two-dimensional digital images created from photographic plates (photographic V band), from the PANBG catalog (Kodaira et al. 1990). The field size is large but the spatial resolution is quite poor ($1''/\text{pixel}$), as is the mean seeing, about $4''$ FWHM. On the other hand, our results were obtained from azimuthally averaged profiles of CCD images with good spatial resolution ($0.3''/\text{pixel}$), much better mean seeing ($\sim 1.45''$ FWHM) but reduced field of view, limiting the maximum profile radius to about $80''$. Therefore, we can expect from BBA data a better disc sampling while our profiles would provide more accurate bulge results.

Due to the differences shown above, in some cases large discrepancies between our results and those from BBA appear, as shown in figure 3.

The sample morphological distribution is shown in figure 2. The results of a χ^2 test on the distribution for the

Table 3. Chi-square test on the morphological distribution for the different nuclear types

Comparison types	χ^2	Significance
S1 vs. S2	2.408	0.992
S1 vs. LINER	8.643	0.799
S1 vs. starburst	29.920	0.005
S1 vs. normal	29.182	0.002
S2 vs. LINER	4.314	0.987
S2 vs. starburst	22.016	0.037
S2 vs. normal	24.120	0.004
LINER vs. starburst	64.457	0.000
LINER vs. normal	38.634	0.000
Starburst vs. normal	96.736	0.000

different nuclear types is presented in table 3. Seyfert 1 and Seyfert 2 galaxies are drawn from the same morphological distribution at 99% confidence level; Seyfert 2 and LINERs are also drawn from the same distribution at nearly 99% confidence level; Seyfert 1 and LINERs follow the same distribution at a lower confidence level ($\simeq 79\%$); on the other hand, the remaining nuclear types present clearly different morphological type distributions. This should be taken into account when analysing the distribution of bulge and disc parameters.

According to HFS, all spiral galaxies show nuclear emission lines. Normal galaxies (with no emission lines in the nuclear spectrum) are only observed in the earliest Hubble types ($T \leq 0$). Most AGNs reside in early-type galaxies (E-Sbc) while starbursts are generally observed in later type galaxies.

As an independent comparison sample, we have added the V and I data from Xanthopoulos (1996) and from Mediavilla et al. (1989). The former sample comprises Seyfert type 1 and 2 galaxies from Véron-Cetty & Véron (2000), with declination between -55° and $+8^\circ$ and redshift $z \leq 0.043$. Hubble types range from -2 (S0) to 5 (Sc); the latter also comprises Seyfert 1 and 2 galaxies from Adams (1977), with redshift $z \leq 0.08$. This sample includes one E galaxy, one N-type galaxy and several disc galaxies with Hubble type ranging from -2 (S0) to 4 (Sbc). This complementary data set comprises 21 Seyfert 1 and 12 Seyfert 2 galaxies.

5.1.2 Disc and bulge parameters

We have performed a statistical analysis on the individual morphological parameter distributions by means of a series of Kolmogorov-Smirnov tests. The results are shown in table 4. It should be recalled that the distribution of morphological types across Seyfert 1, Seyfert 2 and LINER galaxies is quite homogeneous, but that is not true when compared with starbursts and normal galaxies (see table 3). Seyfert 1 and Seyfert 2 effective radii and scale lengths are drawn from the same distribution (*null hypothesis*) at about 97% and 91% confidence level, respectively. On the other hand, while bulges of Seyfert 1 galaxies and LINERs follow the same distribution at about 96% confidence level, disc distributions are most likely different (*null hypothesis* is rejected at 48% confidence level). Seyfert 2 and LINER bulge effective radii are drawn from the same distribution only at less than 70% level, while disc scale lengths follow the same distribution

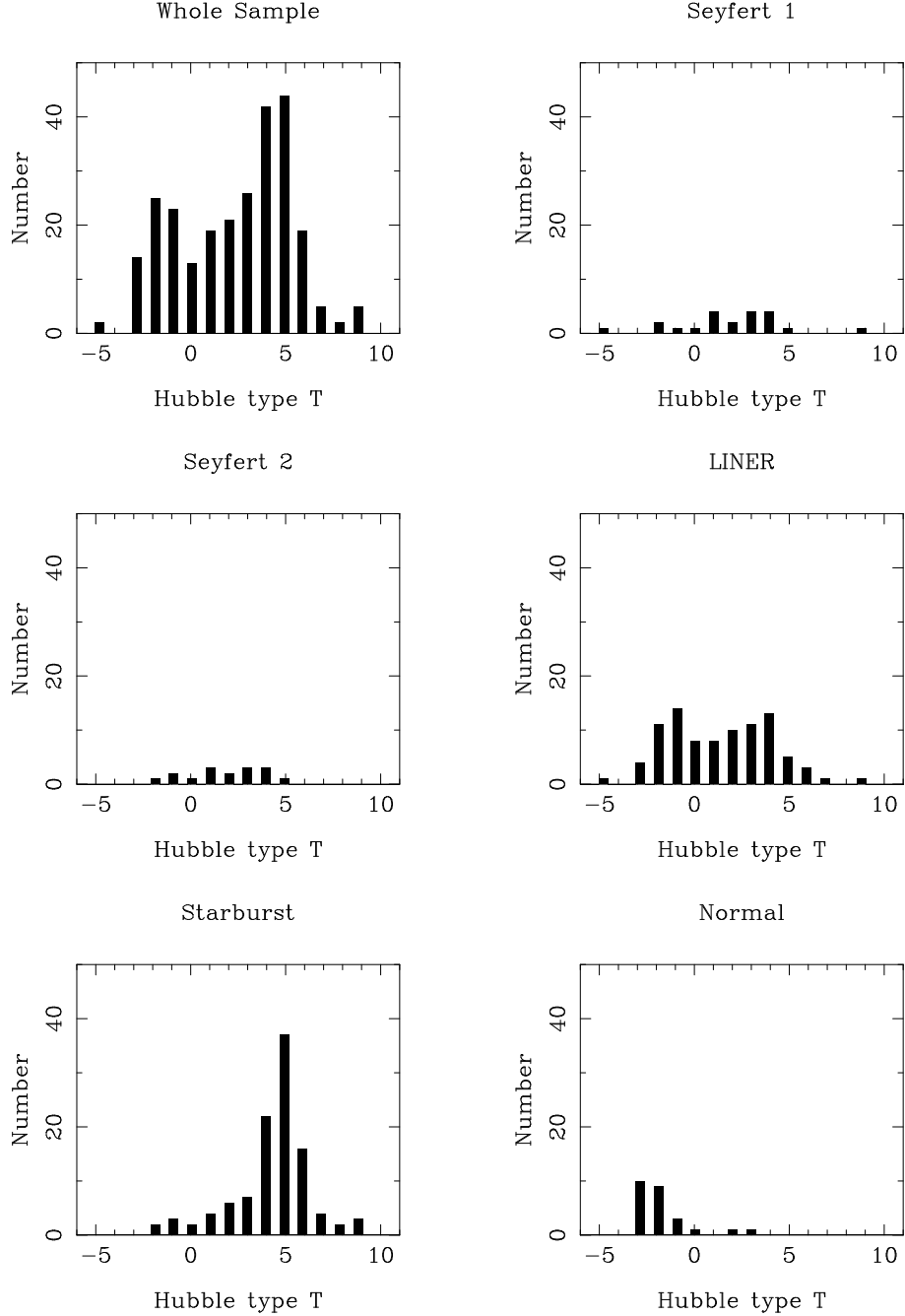


Figure 2. Distribution of morphological Hubble types of the extended sample galaxies

at about 90% level. When comparing active (i.e. Seyfert 1, Seyfert 2 and LINER) galaxies with non-active (i.e. starburst and normal) galaxies, distribution of morphological parameters are generally different (with some exceptions, e.g. disc scale lengths of Seyfert 2 and normal galaxies). As a conclusion, we cannot claim that the individual morphological parameters of active and non-active galaxies follow the same statistical distribution, as other authors do (e.g. Virani et al. 2000).

Perhaps more interesting than the statistics shown above, the distribution of morphological parameters in the $(\mu_0, \log r_0)$ and $(\mu_e, \log r_e)$ planes can be studied. Disc pa-

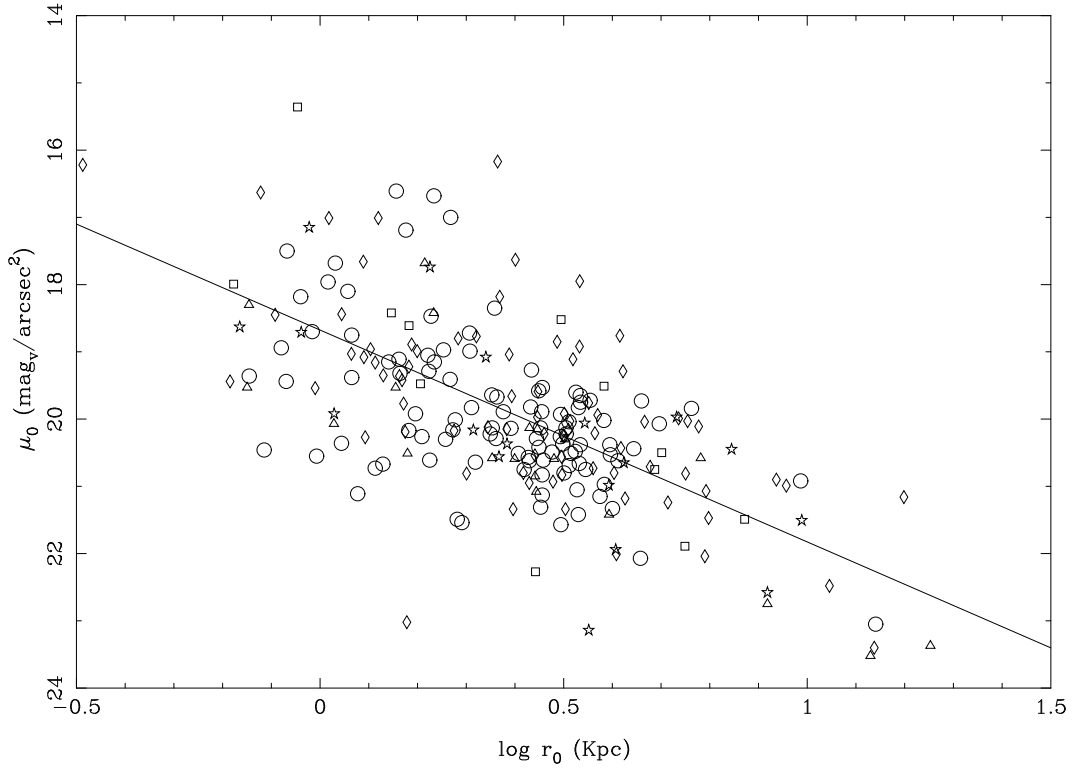
rameters are strongly clustered (perhaps a selection effect due to the luminosity-limited sample) but there is only a weak linear correlation in the $(\mu_0, \log r_0)$ plane, as shown in figure 4.

On the other hand, bulge parameters show a strong linear correlation that constitutes the projection in the $(\mu_e, \log r_e)$ parameter subspace of the “fundamental plane” of ellipticals and bulges of spiral and lenticular galaxies.

We have performed a fit of the relation between bulge parameters μ_e vs. $\log r_e$ by means of linear regression for the different nuclear types. The results are shown in figure 5. We can observe that:

Table 4. Kolmogorov-Smirnov test on the distribution of morphological parameters

Comparison types	K-S	μ_e Significance	K-S	r_e Significance	K-S	μ_0 Significance	K-S	r_0 Significance	K-S	B/D Significance
S1 vs. S2	0.227	0.725	0.148	0.988	0.317	0.440	0.167	0.985	0.245	0.786
S1 vs. LINER	0.127	0.941	0.121	0.961	0.188	0.627	0.188	0.627	0.233	0.356
S1 vs. starburst	0.202	0.489	0.256	0.216	0.211	0.444	0.345	0.037	0.300	0.122
S1 vs. normal	0.280	0.328	0.295	0.269	0.200	0.819	0.250	0.560	0.647	0.001
S2 vs. LINER	0.209	0.596	0.196	0.677	0.267	0.448	0.171	0.921	0.297	0.366
S2 vs. starburst	0.253	0.366	0.275	0.271	0.311	0.248	0.300	0.287	0.445	0.046
S2 vs. normal	0.292	0.388	0.312	0.306	0.433	0.120	0.200	0.925	0.455	0.112
LINER vs. starburst	0.219	0.043	0.266	0.007	0.121	0.522	0.185	0.092	0.402	0.000
LINER vs. normal	0.303	0.063	0.283	0.099	0.288	0.142	0.162	0.792	0.467	0.003
Starburst vs. normal	0.427	0.003	0.250	0.206	0.239	0.293	0.181	0.646	0.847	0.000

**Figure 4.** Disc parameters μ_0 and $\log r_0$ (mag arcsec^{-2} , radii in Kpc). Seyfert 1 galaxies are represented as star symbols (\star), Seyfert 2 as squares (\square), LINERs as diamonds (\diamond), Starbursts as circles (\circ) and normal galaxies as triangles (\triangle). The solid line shown is the result of a linear regression. A weak linear correlation is observed (the correlation coefficient is only about 0.65)

(i) The spheroidal component of starbursts constitutes a lower luminosity class. It is clear in figure 5 that starbursts follow a distribution that lies parallel and below the overall sample. This could be related to the fact that starburst galaxies tend to be late-type galaxies, as is seen in figure 2.

(ii) LINERs and normal galaxies follow very similar distributions (differences in slope are smaller than 0.2σ and $\sim \sigma$ in zero point).

(iii) We can observe differences in the slope of the distributions of Seyfert 1, Seyfert 2, LINERs and normal galaxies. When comparing Seyfert 1 with LINERs and normal galaxies, the differences are of the order σ and can be due to statistical errors. Differences between the Seyfert 2 distribution and that of LINERs and normal galaxies are more significant, $\gtrsim 2.5\sigma$ level. On the other hand, there is a

difference at $\sim \sigma$ level in the slope of the distribution of Seyfert 1 and Seyfert 2 that can be also attributed to statistical uncertainties. Nevertheless, equivalent fits performed in both V and I bands in our comparison sample lead to a very similar result at $\sim 2\sigma$ significance level (see figure 6). Therefore, we have observed that the different classes of galaxies (Seyfert 1, Seyfert 2, LINERs and normal galaxies) show different bulge distributions in the $(\mu_e, \log r_e)$ plane. While sometimes this difference has little statistical significance, in the case of Seyfert 2 galaxies it is more important, since it cannot be solely attributed to statistical effects. If real, the observed distribution difference could imply families of bulges with *different* physical properties, as proposed for bright and faint cluster ellipticals (Hoessel et al. 1987). Capaccioli et al. (1992) also describe two physically different

families of ellipticals, early type dwarfs and bulges of SOs and spirals, each family described by a different relation in the $(\mu_e, \log r_e)$ plane. One of the families comprises the cluster brightest cD and quasar-hosting galaxies, while the other comprises normal ellipticals, fainter bulges and early type dwarfs. According to these authors, the latter objects are in the latest stages of dissipative collapse, while the former ones have experienced merging and accretion processes.

The stellar kinematics in the nuclei of Seyfert galaxies both of types 1 and 2 seems to be similar to that in normal galaxies, with active and non-active galaxies following the same Faber-Jackson relation (Terlevich, Diaz & Terlevich 1990; Nelson & Whittle 1996). Further evidences on the similarity of stellar kinematics in active and normal galaxies has been provided by Ferrarese et al. (2001). They studied the $M_\bullet - \sigma$ relation for AGNs, an empirical correlation between the central black hole mass and the stellar velocity dispersion, finding a good agreement between black hole masses derived from reverberation mapping and from the $M_\bullet - \sigma$ relation as derived from normal and weakly active galaxies, indicating a common relationship between active and quiescent black holes and their host galaxy environment. Regarding gas motions the relation between the velocity dispersion of the gas in the NLR and the stellar velocity dispersion and for galaxies of Seyfert types 1 and 2 shows a large scatter although clustered around the 1:1 line (Jiménez-Benito et al. 2000). This suggests that gas motions are mainly controlled by the mass of the galactic bulge along with other agents, like shock waves that may be produced by the interaction of jets with ambient gas, or tidal interactions with companions, providing an additional line broadening. Yet, the kinematics of the two main types of Seyfert galaxies show some differences that need to be explained: a ratio between gas and stellar velocity dispersions larger than one is common in Seyfert type 2 nuclei, while some Seyfert type 1 nuclei show emission lines which are narrower than the stellar absorption lines.

5.1.3 Type II discs

As shown in section 4.1 we have found type II discs in three Seyfert galaxies and in one LINER from our original sample. Since no type II disc was detected in non-active (i.e. starburst or normal) galaxies, we have investigated the possible connection between nuclear activity and the existence of type II discs. The BBA sample parameters were derived using the modified Kormendy function (equation 3) and a large fraction of the objects ($\simeq 50\%$) presents a type II disc.

Tables 5 and 6 show the statistics of type II discs in the extended sample. As shown in table 5, we don't find correlation between the existence of type II discs and nuclear activity. In fact, the highest fraction of type II discs is found in normal galaxies. Nevertheless, we do find a greater incidence of type II discs in earlier morphological types ($T = -3$ to $T = 0$) as shown in table 6.

5.1.4 B/D relation

We have derived the B/D relation by means of equation 6. As comparison values, we have used the mean values obtained by Simien & de Vaucouleurs (1986) (hereafter SDV);

Table 5. Type II discs vs. nuclear type

Nuclear type	No. of objects with disc fit	No. of objects with type II disc	Ratio (%)
Seyfert 1	19	6	31.6
Seyfert 2	12	4	33.3
LINER	80	31	38.7
Starburst	103	24	23.3
Normal	20	8	40.0

Table 6. Type II discs vs. Hubble type

Hubble type T	No. of objects with disc fit	No. of objects with type II disc	Ratio (%)
-3	11	6	54.5
-2	21	9	42.9
-1	21	11	52.4
0	12	6	50.0
1	16	3	18.7
2	19	3	15.8
3	25	7	28.0
4	38	10	26.3
5	41	14	34.1
6	19	4	21.0

these values served as a reference data set, rejecting all morphological parameters leading to B/D values highly deviated from SDV data. Nevertheless, it is worth mentioning that SDV B/D values present a large scatter, mainly attributed to errors in the surface photometry and in the decomposition process and, to a lesser extent, to morphological classification errors.

The distribution of B/D values is shown in figure 7 (left pannel). As can be observed in table 4, the B/D relation values for Seyfert 1 and Seyfert 2 galaxies are drawn from the same distribution and 86% confidence level. On the other hand, Seyfert and LINER B/D distributions are most likely different since null hypothesis is rejected at about 26% and 37% confidence level for Seyfert 1 and Seyfert 2, respectively.

As can be observed in figure 7 and in the mean deviation estimators shown in table 7, B/D values spread over a large range, specially for the earliest morphological types ($T < 0$). In order to avoid the effects of outliers, we have used the median $(B/D)_{median}$ rather than the mean as a robust average estimator. As shown in table 7 and in the right pannel of figure 7, a descending trend is observed in $(B/D)_{median}$ with the Hubble type T, as expected from the definition of the latter as a sequence of decreasing importance of the spheroidal component with respect to the disc. This trend is also reflected in SDV data. Our median values are generally higher than those derived by SDV (see table 7); this can be at least partially explained by the fact that we allow for the existence of type II discs (not considered by SDV); on the other hand, SDV values are derived from the B band while ours are computed from V band surface profiles. From table 7 and figure 7 we can observe that:

- (i) The distribution of $(B/D)_{median}$ seems to be generally independent of the nuclear type.
- (ii) Nevertheless, for the earliest morphological types ($T < 0$), Seyfert galaxies tend to have a higher $(B/D)_{median}$

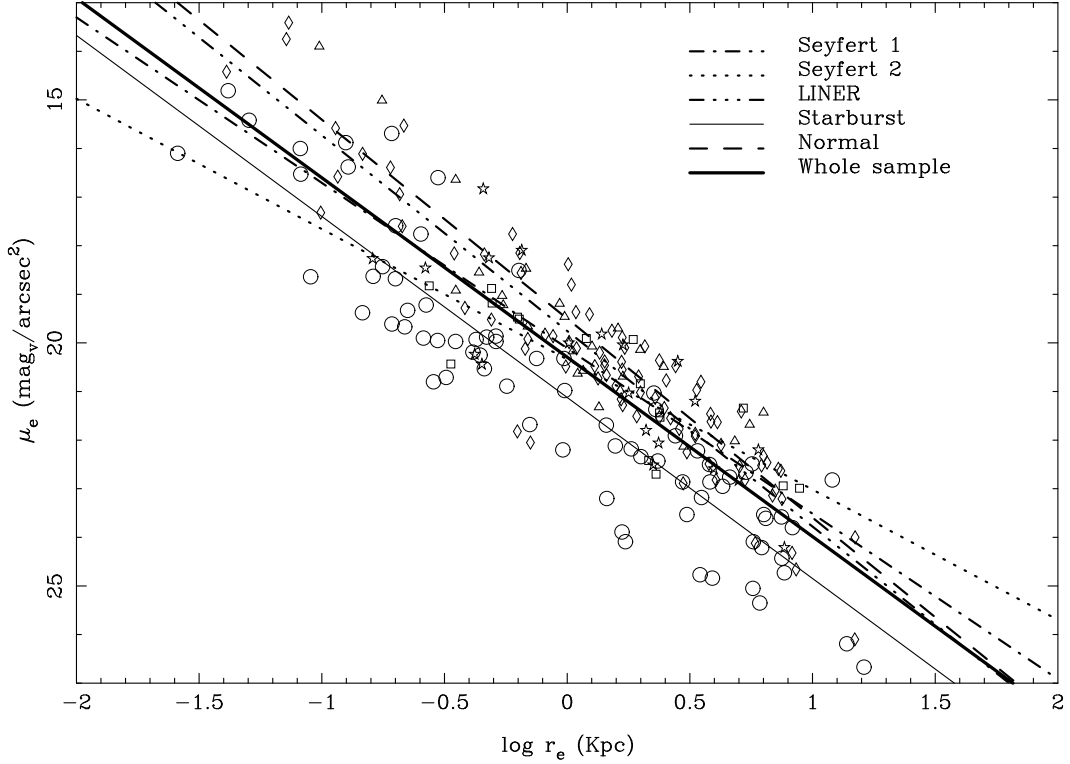


Figure 5. Bulge parameters μ_e and $\log r_e$ (mag arcsec^{-2} , radii in Kpc). Symbols as in figure 4. Regression lines have been plotted for all nuclear types.

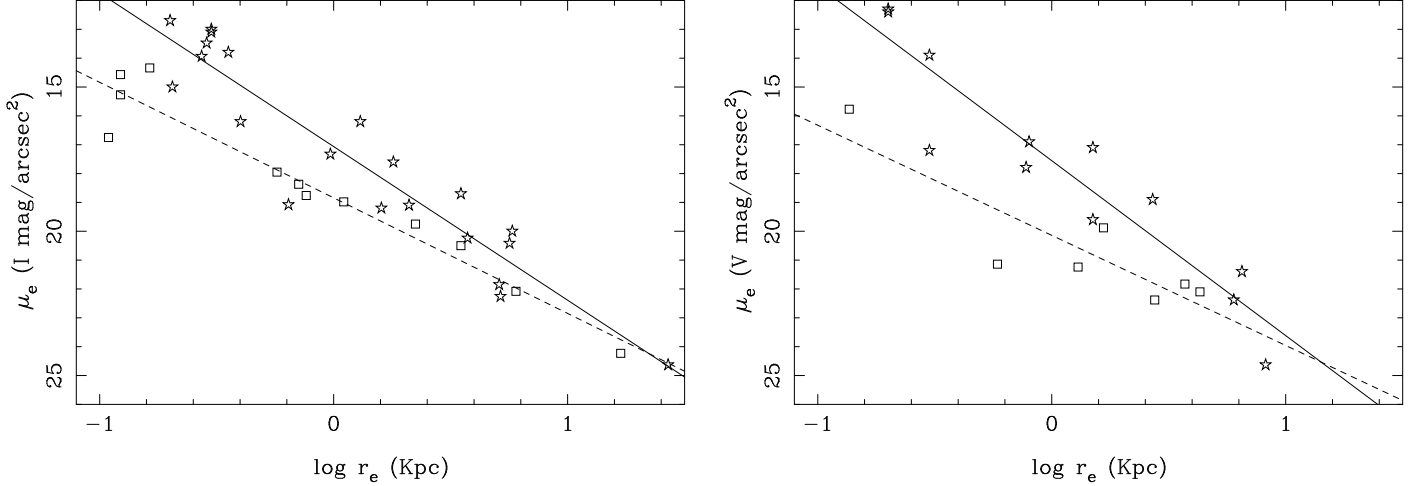


Figure 6. Bulge parameters μ_e and $\log r_e$ (mag arcsec^{-2} , radii in Kpc) for the comparison sample in the I (left) and V bands. Symbols as in figure 4. The solid line corresponds to the linear regression for Seyfert 1 galaxies and the dashed line to Seyfert 2 galaxies. Differences in the slope of both distributions are $\simeq 2.4\sigma$ in the I band and $\simeq 1.9\sigma$ in the V band.

relation (greater relative importance of the spheroidal component) than the remaining types.

(iii) Starburst galaxies show smaller $(B/D)_{\text{median}}$ values than the remaining nuclear species for the earliest Hubble types ($T < 0$) and approximately constant between $T = -1$ and $T = 3$.

(iv) From $T = 1$ onwards, $(B/D)_{\text{median}}$ is quite uniform across all nuclear types.

5.2 Radial colour distribution

Yee (1983) performed Gunn r , g , v surface photometry on a sample of twenty Seyfert galaxies from the Markarian catalog concluding that the colours of the underlying galaxies are comparable to those of normal spirals in the Sa-Sbc range, but the nuclear colours are bluer in Seyfert 1 galaxies than in Seyfert 2 objects. Xanthopoulos (1996) performed aperture photometry on a sample of 27 Seyfert 1 and Seyfert 2 galaxies using 2.5, 5, 10 and 20 Kpc apertures. No differ-

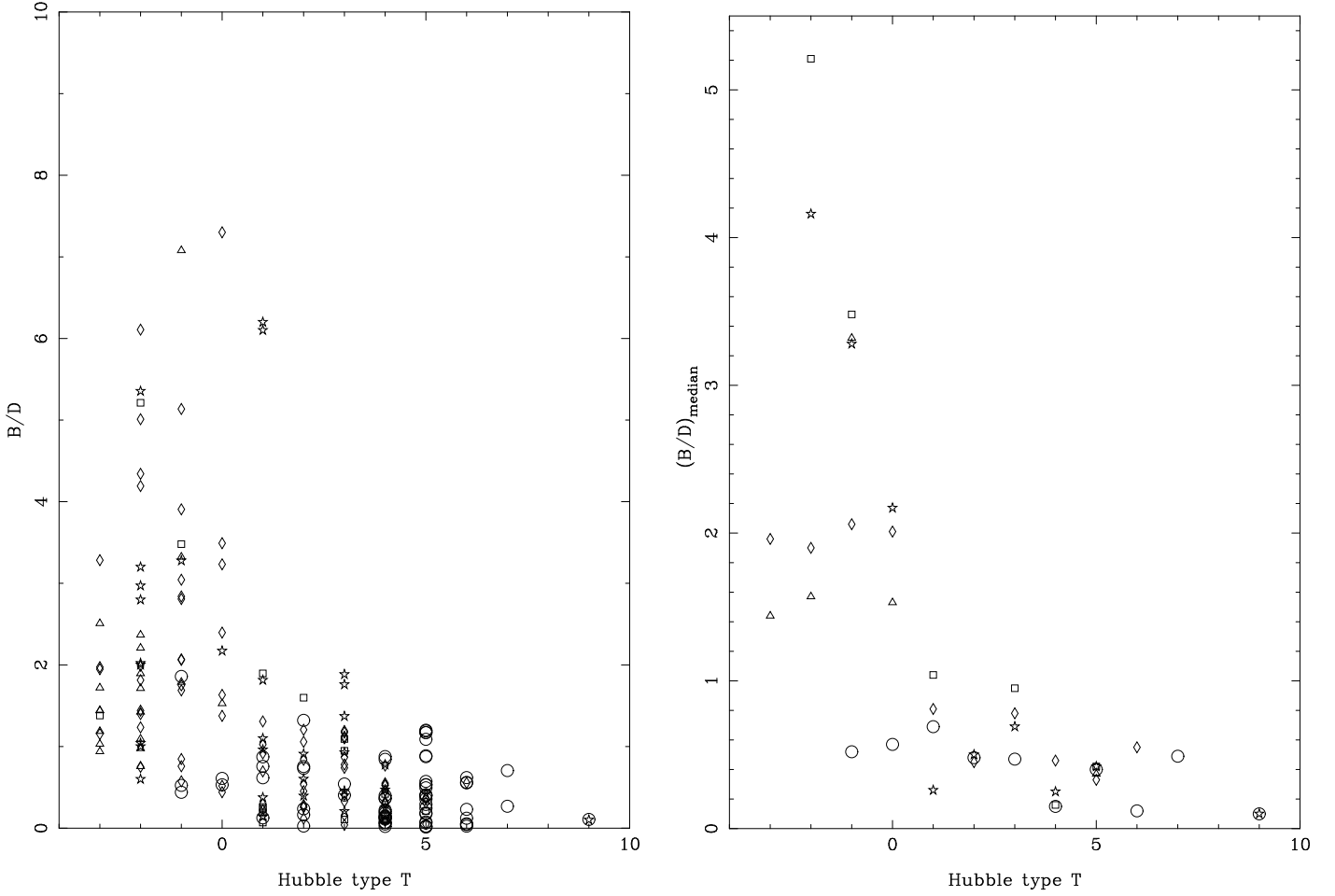


Figure 7. Distribution of B/D relation (left panel) and median value $(B/D)_{median}$ (right panel) for the different morphological types. Symbols as in figure 4.

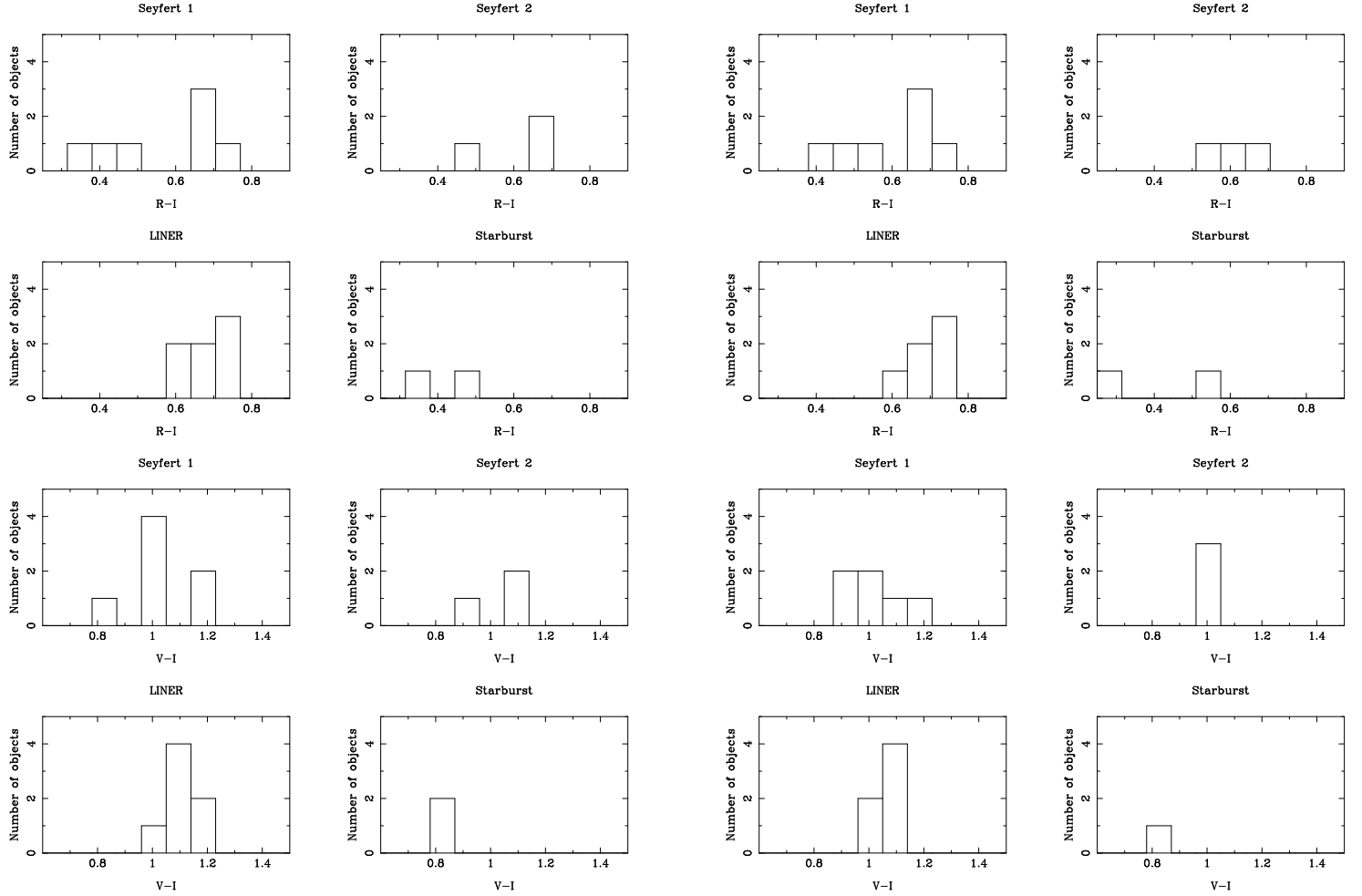
Table 7. Median B/D relation vs. morphological type. SDV mean B/D values are shown for comparison

Hubble type T	No. of objects	$(B/D)_{median}$	mean dev.	$\langle B/D \rangle$ (SDV)	mean dev. (SDV)
-3	11	1.44	0.52	1.43	0.42
-2	21	1.89	1.29	1.33	0.24
-1	20	2.06	1.23	1.27	0.32
0	12	1.58	1.27	1.02	0.13
1	16	0.66	0.45	0.55	0.32
2	18	0.49	0.36	0.48	0.10
3	20	0.76	0.38	0.29	0.05
4	33	0.25	0.19	0.22	0.06
5	29	0.40	0.29	0.11	0.02
6	10	0.18	0.22	0.04	0.01
7	2	0.49	0.22	0.02	0.01
8	-	-	-	-	-
9	2	0.10	0.003	-	-

ences (within the measurement uncertainties) were found in the $V - R$, $R - I$ and $V - I$ colours in the 10 and 20 Kpc apertures characterizing the disc. In the 2.5 Kpc and 5 Kpc apertures, however, the $R - I$, and, to a lower degree, the

$V - I$ colours appear bluer in Seyfert 1 galaxies than in Seyfert 2.

It should be taken into account that AGN aperture photometry is contaminated by nuclear emission lines and it is expected that this effect would be more noticeable in the smaller diaphragms. This is specially true for the $R - I$ colour in Seyfert 1 galaxies, since the R band contains the broad component of H_{α} . $R - I$ colours are then expected to be bluer in Seyfert 1 galaxies than in Seyfert 2 ones. Since we are interested in characterising the underlying galaxy colours, we would need to parametrise them avoiding the nuclear emission lines. To this end, we have used the radial colour distributions presented in Paper I, analysing the $R - I$ and $V - I$ colour profiles. While radial distributions of bulges and discs generally become bluer outward (Balcells & Peletier, 1994), gradients are small enough that it is possible to assign representative values for the colour of each component. For instance, Peletier & Balcells (1996) selected as characteristic of bulges the colour at $0.5 \times r_e$ or at 5 arcsec, whichever is larger, and for discs the colours at $2 \times r_0$. In order to minimise the risk of nuclear contamination at small radii in bulges and too high colour errors at large radial distances in discs, we have decided to select as representative the colours at effective radius (r_e) for bulges and those at scale length (r_0) for discs.

**Figure 8.** Distribution of bulge (left) and disc characteristic colours

The results are somewhat qualitative, since statistics are not reliable for such a small sample. As shown in figure 8, we have found that the range of characteristic bulge and disc colours is comparable in all nuclear types, albeit mean bulge and disc characteristic colours are bluer in Seyfert galaxies than in LINERs. Seyfert 1 bulge and disc characteristic colours are somewhat bluer than those of Seyfert 2. Nevertheless, it should be taken into account that the bluest Seyfert 1 observed bulge colours are almost certainly contaminated by either the NLR component (NGC 3227) or by circumnuclear star-forming rings (NGC 3982 and NGC 7469).

As a first comparison, we have represented in figure 9 our bulge and disc colours along with photoelectric photometry values of standard stars from Moreno & Carrasco (1986) and Graham (1982) and aperture photometry of early-type galaxies from Poulain (1988). We have also included colours from population synthesis models computed by Bressan et al. (1994) at $Z = Z_{\odot}$ and $Z = 2.5Z_{\odot}$ and a large range of ages (from 6.3×10^6 to 19.95×10^9 years). There is an acceptable agreement between our colours and those of the comparison sample: they are comprised between those derived from aperture photometry of early-type galaxies (whose colours are generally redder) and the population synthesis models.

A further step is the comparison of our characteristic

colours with those of normal galaxies with similar morphological type. To this end, we have selected a reference sample of 18 early-type galaxies (Balcells & Peletier, 1994; Peletier & Balcells, 1996). Those studies will be referenced hereafter as BP). Three of them are catalogued as normal galaxies in HFS, while four of the galaxies have been labelled as transition types or LINERs. The remaining eleven objects are not included in the HFS sample, but have been checked in NED and in Véron-Cetty & Véron (2000) for the absence of active nucleus.

Characteristic colours from BP have been derived from colour gradients rather than from the colour profiles themselves. These authors find that bulge colours are predominantly bluer than those of elliptical galaxies, but both bulges and ellipticals follow the same sequence in the colour-colour diagram. They conclude that stellar populations of bulges must be similar to those of elliptical galaxies, but the former, as a class, have lower metallicities and larger spread in ages than giant ellipticals. Visvanathan & Sandage (1977) found that ellipticals and S0 galaxies follow a colour-magnitude relation in which brighter galaxies are redder; BP also tried to correlate bulge colours and global galaxy parameters. They find that the (weak) correlation between colours and absolute magnitude improves slightly when the total galaxy luminosity is used instead of the bulge luminosity alone.

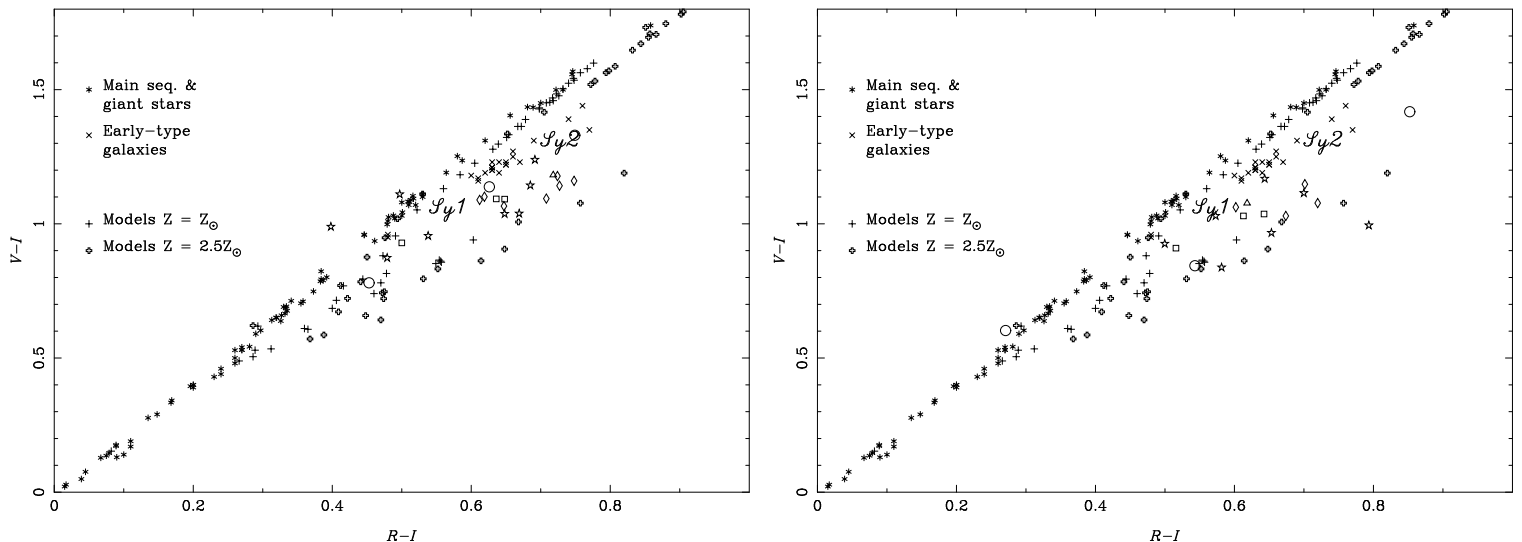


Figure 9. Bulge (left) and disc (right) characteristic colours compared with photoelectric photometry of stars and early-type galaxies and with population synthesis-derived colours. Symbols as in figure 4. The points labelled as *Sy1* and *Sy2* correspond to the mean Seyfert 1 and Seyfert 2 colours in the 5 Kpc aperture from Xanthopoulos (1996).

This might indicate that the total galaxy potential, and not the bulge alone, determines the chemical enrichment of the bulge. Moreover, they find that bulge and disc colours derived from profiles are very similar, suggesting that the bulk of the inner disc and bulge stars are essentially coeval. At most, disc stars are 2-3 Gyr younger than bulge stars.

Figure 10 shows the relationship between our characteristic $R - I$ colours and the bulge, disc and total galaxy luminosity. BP data have also been plotted in order to compare the control sample colours with ours. We find that:

- (i) When comparing our sample with the control sample, we find a very similar colour range; this is true for both bulge and disc components and may suggest that the bulge and disc stellar populations (ages and metallicities) are comparable in normal and active galaxies.
- (ii) We confirm the result from BP that bulges and disc characteristic colours derived from profiles are very similar, though there is a wider range of disc characteristic colours.
- (iii) We are not able to confirm a correlation between bulge colours and bulge luminosity. Moreover, this situation does not improve when using the total galaxy luminosity instead of the bulge luminosity alone.

6 CONCLUSIONS

We have investigated the main structural properties derived from VRI and $H\alpha$ surface photometry of galaxies hosting nuclear emission-line regions (including Seyfert 1, Seyfert 2, LINER and starburst galaxies) as compared with normal galaxies. Our original sample is thoroughly described in Paper I and comprises 21 active galaxies, 3 starbursts and 1 normal galaxy. For our investigation on bulge and disc parameter distributions, we have extended the sample up to 261 objects hosting all levels of nuclear activity (ranging from normal to Seyfert 1 galaxies). Our study has found several differences between the structural parameters of active

and non-active galaxies. From the statistical analysis performed in section 5.1.2, we cannot claim that the individual morphological parameters of active and non-active galaxies follow the same statistical distribution. On the other hand, we have studied the distribution of morphological parameters in the $(\mu_0, \log r_0)$ and $(\mu_e, \log r_e)$ planes. Disc parameters are found strongly clustered (perhaps a selection effect) but the linear correlation is weak. On the other hand, there is a strong linear correlation of bulge parameters. We have studied the distributions across the different nuclear types, finding that starbursts constitute a lower luminosity bulge class. LINERs and normal galaxies follow very similar distributions. Seyfert 1, Seyfert 2 and LINERs follow different distributions at statistically significant level. These differences could perhaps imply families of bulges with different physical properties. Type II discs are analysed in section 5.1.3. We don't find a correlation between type II discs and nuclear type but with Hubble type. B/D relation is studied in section 5.1.4. We find that the distribution of $(B/D)_{median}$ seems to be generally independent of the nuclear type, except for the earliest ($T < 0$) Hubble types. Finally, bulge and disc characteristic colours derived from radial profiles have been investigated in section 5.2. We find that the range of characteristic bulge and disc colours is comparable in all nuclear types, though mean bulge and disc colours are bluer in Seyfert galaxies than in LINERs. Nevertheless, this result is uncertain since bulge colours can be affected by line emission contamination arising from the NLR and/or circumnuclear star-forming regions. When comparing our characteristic bulge and disc colours with those of the control sample of early-type galaxies, we find a very similar colour range that may suggest that the bulge and disc stellar populations are comparable in normal and active galaxies. On the other hand, we find that bulges and disc characteristic colours derived from profiles are very similar. We don't detect a correlation between bulge colours and bulge or total galaxy luminosities.

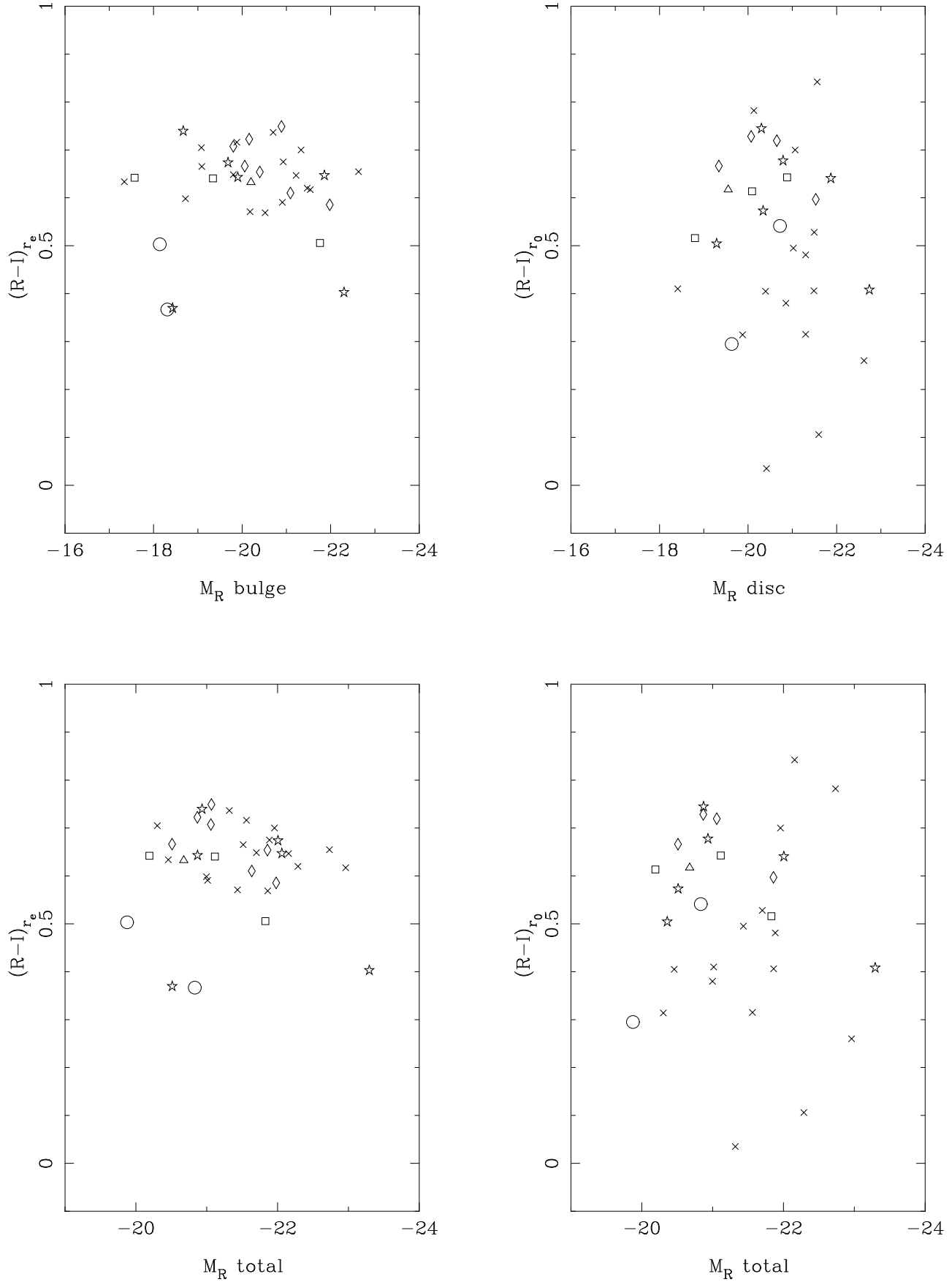


Figure 10. Sample bulge (left diagrams) and disc (right diagrams) characteristic colours (symbols as in figure 4) plotted against bulge, disc and total absolute magnitudes. The comparison sample (\times symbols) comprises 18 early-type galaxies from Balcells & Peletier (1994) and Peletier & Balcells (1996).

ACKNOWLEDGMENTS

The JKT is operated on the island of La Palma by the Isaac Newton Group in the Spanish Observatorio del Roque de los Muchachos of the Instituto de Astrofísica de Canarias. We would like to thank CAT for awarding observing time. We also thank an anonymous referee for suggestions that greatly improved the clarity of the paper. This research has made use of the NASA/IPAC Extragalactic Database (NED) which is operated by the Jet Propulsion Laboratory, California Institute of Technology, under contract with the National Aeronautics and Space Administration. M. Sánchez would like to thank Isabel Casanova for her assistance entering and revising the large amount of data from the literature. This work has been partially supported by DGICYT project AYA-2000-0973.

REFERENCES

- Adams T.F., 1977 ApJS, 33, 19
- Andredakis Y.C., Peletier R.F., Balcells M., 1995, MNRAS, 275, 874
- Baggett W.E., Baggett S.M. & Anderson K.S.J., 1998, AJ, 116, 1626
- Balcells M., and Peletier R.F., 1994, AJ, 107, 135
- Boris N.V., Donzelli C.J., Pastoriza M.G., Rodríguez-Ardila A., Ferreira D.L., 2002, A&A, 348, 780
- Borson T., 1981, ApJS, 46, 177
- Bressan A., Chiosi C. & Fagotto F., 1994, ApJS, 94, 63
- Capaccioli M., de Vaucouleurs G., 1983, ApJS, 52, 465
- Capaccioli M., Caon N. & D’Onofrio M., 1992, MNRAS, 259, 323
- Carollo C.M., Stiavelli M., Mack J., 1998, AJ, 116, 68
- Carone T. E., 1992, In: Filippenko A. V. (ed) Relationships between Active Galactic Nuclei and Starburst Galaxies. ASP Conf. Ser., 31, 375
- Díaz A. I., Álvarez M., Terlevich E., Terlevich R., Sánchez-Portal M., Aretxaga I., 2000, MNRAS, 311, 120
- de Jong R. S., 1996, A&AS, 118, 557
- de Vaucouleurs G., de Vaucouleurs A., Corwin H. G. Jr., Buta R., Paturel G. & Fouqué P., 1991, Third Reference Catalog of Bright Galaxies. New York: Springer (RC3)
- de Vaucouleurs G., 1948, Ann. d’Ap., 11, 247
- Ferrarese L., Pogge R.W., Peterson B.M., Merritt D., Wandel A., Joseph C.L., 2001, ApJ, 555, L79
- Freeman K. C., 1970, ApJ, 160, 811
- Freeman K. C., 1976, in: Proceedings of the Sixth Advanced Course, Saas-Fee, Switzerland
- Graham J. A., 1982, PASP, 94, 244
- Ho L. C., Filippenko A. V., Sargent W. L. W., 1997, ApJS, 112, 315 (HFS)
- Hoessel J.G., Oegerle W.R. & Schneider D.P., 1987, AJ, 94, 1111
- Hunt L. K., Giovanardi C., 1992, AJ, 104, 1018
- Hunt L. K., Malkan M. A., Salvati M., Mandolesi N., Palazzi E., Wade R., 1997, ApJS, 108, 229
- Hunt L. K., Malkan M. A., Moriondo G., Salvati M., 1999, ApJ, 510, 637
- Jiménez-Benito L., Díaz A. I., Terlevich R. J., Terlevich E., 2000, MNRAS, 317, 907
- Kent S. M., 1985, ApJS, 59, 115
- Kodaira K., Okamura S., Ichikawa S., 1990, Photometric Atlas of Northern Bright Galaxies. University of Tokyo Press
- Kormendy J., 1983, In: Proceedings of the Twelfth Advanced Course, Saas-Fee, Switzerland
- Kormendy J., 1977, ApJ, 217, 406
- MacKenty J. W., 1990, ApJS, 72, 231
- Márquez I., Durret F., González Delgado R.M., Marrero I., Masegosa J., Maza J., Moles M., Pérez E. & Roth M., 1999, A&AS, 140, 1
- Márquez I., Durret F., Masegosa J., Moles M., González Delgado R.M., Marrero I., Maza J., Pérez E. & Roth M., 2000, A&A, 360, 431
- Márquez I., Moles M., 1994, AJ, 108, 90
- Mediavilla E., Pastoriza M.G. & Battaner E., 1989, Ap&SS, 157, 145
- Moreno H., Carrasco G., 1986, A&AS, 65, 33
- Mulchaey J. S., Regan M. W. & Kundu A., 1997, ApJS, 110, 299
- Mulchaey J. S. & Regan M. W., 1997, ApJ, 482, L135
- Nelson C. H. & Whittle M., 1996, ApJ, 465, 96
- Pastoriza M.G., Mediavilla E., Battaner E., 1989, in: Osterbrock D. E., Miller J. S. (eds.) IAU Symposium 134, Active Galactic Nuclei. Dordrecht: Kluwer
- Peletier R. F. & Balcells M., 1996, AJ, 111, 2238
- Poulain P., 1988, A&AS, 72, 215
- Sánchez Portal M., Díaz A. I., Terlevich R., Terlevich E., Álvarez M., Aretxaga I., 2000, MNRAS, 312, 2 (Paper I)
- Schombert J. M., Bothum G. D., 1987, AJ, 92, 60
- Sérsic J.L., 1968, Atlas de Galaxias Australes (Córdoba: Observatorio Astronómico)
- Shlosman I., Begelman M., Frank J., 1989, Nature, 338, 45
- Simien F. & de Vaucouleurs G., 1986, ApJ, 302, 564 (SDV)
- Terlevich E., Díaz A. I., Terlevich R. J., 1990, MNRAS, 242, 271
- Terlevich R.J., Sánchez-Portal M., Díaz A. I., Terlevich E., 1991, MNRAS, 249, 36
- Véron-Cetty M.-P. & Véron P., 1993, A Catalogue of Quasars and Active Nuclei; ESO Scientific Report #13 (6th edition)
- Véron-Cetty M.-P. & Véron P., 2000, A Catalogue of Quasars and Active Nuclei; ESO Scientific Report #13 (9th edition)
- Virani S.N., De Robertis M.M. & VanDalsen M.L., 2000, AJ, 120, 1739
- Visvanathan N., & Sandage A., 1977, ApJ, 216, 214
- Xanthopoulos E., 1996, MNRAS, 280, 6
- Yee H. K. C., 1983, ApJ, 272, 473

This paper has been produced using the Royal Astronomical Society/Blackwell Science L^AT_EX style file.